Részletes szakmai beszámoló a T043287 OTKA pályázathoz

1. Atomi rendszerek kvantumállapotának kontrollja

Szuperponált állapotok robusztus keltése

Napjainkra számos olyan jelenséget fedeztek fel, amely atomi rendszerek belső energiaszintjeinek koherens szuperponált állapotain alapulnak. Szuperponált állapotok létrehozására egyik legkézenfekvőbb módszer az atom kvantumállapotának közel rezonáns fényimpulzusokkal történő kontrollja. Az OTKA pályázat keretében olyan atomi rendszereket vizsgáltunk, amelyekben egy vagy több atomi energiaszint degenerált, ennélfogva általában az egyes atomi állapotpárokat (alap és gerjesztett állapotok) nem lehet egymástól függetlenül csatolni. Ilyen körülmények között annak érdekében, hogy a degenerált rendszer előre meghatározott végállapotba kerüljön kvantuminterferencia jelenségeket kell kihasználni. A kidolgozott kontroll folyamatok többségében a rendszer kiindulási állapotát ismertnek tételeztük fel, de bemutattunk olyan sémát is, ahol a végállapot független a kezdőállapottól.

Két degenerált energiaszinttel rendelkező rendszer kvantumállapotának kontrollját mutattuk be az [1] közleményben. A degeneráció tipikus forrása az, hogy az atomi energiasajátállapotok egyben impulzusmomenum sajátállapotok is. A bemutatott sémában elliptikusan polarizált $n\pi$ területű impulzussal kell megvilágítani az atomokat, melyek több Rabi oszcillációt követően jutnak el a kívánt végállapotba. Ezzel a módszerrel a rendszer lehetséges végállapotainak csak egy részhalmazát lehet preparálni. A cikkben közölt sémát továbbfejlesztve három szintes, degenerált rendszer adiabatikus, koherens kontrollját ismertettük a [2] publikációban. Módszerünk az ún. STIRAP (Stimulated Raman Adiabatic Passage) eljáráson alapul, melyet eredetileg három atomi állapotból álló rendszerre dolgoztak ki. Az adiabatikus módszerek nagy előnye a Rabi oszcilláción alapulókkal szemben az, hogy robosztusak az alkalmazott fényimpulzusok területének és időzítésének fluktuációival szemben. Az általános módszert alkalmaztuk a metastabil He atomra a [3] publikációban. A kidolgozott adiabatikus kontroll folyamatokat a [4] cikkben foglaltuk össze.

Az eddig ismertetett eljárások koherens folyamatokon alapulnak és koherens szuperponált állapotok preparálására alkalmasak. Kevert állapotokat viszont nem lehet előállítani koherens folyamatokkal a disszipáció hiánya miatt. A [5] munkában megmutattuk, hogy egy kétdimenziós sötét altérrel rendelkező négy szintű atomi rendszerben koherens és inkoherens folyamatok kombinálásával, a STIRAP módszerrel rokon módon állapotok tervezhetők a rendszer három degenerált alapállapota által kifeszített térben. A két sötét altér helyzete a külső lézerekkel változtatható, és egy előírt tiszta, vagy speciálisan kevert célállapothoz mindig található olyan helyzetük, hogy az állapot a sötét altérbe essen. Ezt kihasználva sorozatos sötét altér változtatással és a disszipáció figyelembe vételével tetszőleges kiindulási állapot az előírt célállapotba juttatható nagy pontossággal. A rendszer végállapota a koherens gerjesztő lézerek által meghatározott sötét altérben található, így további disszipáció nem történik. A tervezhető állapotok köre bővebb, mint a hagyományos módszerek esetében, mivel a kevert állapotok egy tág osztálya is pontosan előállítható. Megmutattuk, hogy annak ellenére, hogy a módszer nem adiabatikus, mégis robusztus: nem érzékeny az alkalmazott impulzusok területére vagy időzítésére, csak azok arányára; valamint a spontán

emisszió miatti populációveszteség is kompenzálható egy pumpa lézer alkalmazásával.

A publikált koherens kontroll sémák több alkalmazását kidolgoztuk. A kvantuminformatikai alkalmazásokat külön fejezetben mutatjuk be. A következő alfejezetben egy molekulafizikai probléma megoldására tett javaslatot ismertetünk.

Királis molekulák konverziója

Számos molekulának több térbeli konfigurációja is lehetséges, azaz a molekulát alkotó atommagok egy olyan potenciálfelületen helyezkednek el, amelynek több minimuma is van. Az ilyen típusú molekulák egy része királis tulajdonságú, azaz képes a fény polarizációjának forgatására. A molekulafizikában fontos kérdés, hogyan lehet a molekulákat a különböző térbeli konfigurációk között külső kölcsönhatással átvinni. Javasoltunk [6] egy egyszerű, koherens fénnyel megvalósítható forgatást, amellyel egy molekula két királis állapota között lehet váltogatni.

Nyílt rendszerek időfejlődésének leírása

A különböző fizikai rendszereken implementált elemi kvantumkapuk műveleti pontatlansága és az elkerülhetetlenül fellépő disszipációs folyamatok meggátolják nagy hálózatok építését. A pontatlanság és disszipáció mértékére létezik egy felső korlát, ami alatt lehetővé válik tetszőleges mértékben hibatűrő kvantumszámítógép építése. A disszipáció és pontatlanság teljes jellemzéséhez az időfejlesztő operátor meghatározása szükséges.

E célból eljárást dolgoztunk ki [7] nyílt kvantumrendszerek időfejlesztő operátorának sztochasztikus operátorösszeg reprezentációban történő meghatározására. A kidolgozott módszer lényege, hogy a kvantumtrajektória módszerek tulajdonságait felhasználva az időfejlesztő operátor egy megnövelt Hilbert téren ható sűrűségoperátorral azonosítható, és e sűrűségoperátor trajektóriák átlagolásával megkapható. Az eredmény lehetővé teszi, hogy egyszerre nagyszámú kiindulási állapot időfejlődését hatékonyan meghatározzuk – a kiindulási állapotok alterének dimenziójával arányosan rövidebb idő alatt, mintha külön-külön tekintenénk a kiinduló állapotok fejlődését. A módszer előnyeit és működési elvét egy üregrezonátorba helyezett kétatomos rendszerrel megvalósított kontrollált-nem kapun mutattuk be, valamint meghatároztuk a kvantumkapu műveletvégzésének hűségét a disszipációt leíró paraméterek függvényében.

A kísérletekben nem lehet közvetlenül meghatározni egy rendszer időfejlesztő operátorát. Ezzel szemben a rendszerre jellemző kétidős korrelációs függvények jól mérhető mennyiségek, így a mérési eredményeket össze lehet vetni a rendszer fizikai modelljével. Ennek érdekében számítási eljárást dolgoztunk ki kétidős korrelációs függvények meghatározására [8]. Eljárásunk alapja az, hogy a korrelációs függvényben szereplő operátor szorzatot egy sűrűségoperátor bázis bevezetésével szétválasztjuk két független részre. E két rész felel meg a szorzatban szereplő operátorok Heisenberg-képben vett reprezentációjának. Az eljárás hatékonyan alkalmazható kis dimenziós, a kvantumtrajektória módszerek valamelyikével numerikusan számított időfejlődésű rendszerekben, amennyiben a kiszámítandó különböző korrelációs függvények száma a rendszer dimenziójának négyzetével összemérhető. Numerikus példán keresztül megmutattuk, hogy egy két dimenziós rendszer esetén egyszerre három korrelációs függvény számítása a bemutatott módszerrel hatékonyabb, azaz rövidebb idő alatt érhető el ugyanakkora pontosság, mint a standard, az irodalomban gyakran használt

számítási módszerrel. Az eljárás elvi érdekessége, hogy Heisenberg-képbeli operátorok olyan reprezentációját adja, amelyből a korrelációs függvény értékei egyszerű skaláris szorzással megkaphatók.

Degenerált rendszerek kvantumállapotának rekonstrukciója

A különféle kontroll sémák sikeres „működéséről" mérésekkel lehet meggyőződni. Amennyiben a mérések során a rendszerről gyűjtött adatokból a rendszer kvantumállapotát teljes egészében meg lehet határozni, úgy kvantumállapot rekonstrukcióról beszélünk. Kidolgoztunk egy rekonstrukciós eljárást $J = 2$ teljes impulzusmomentumú energiasajátállapot $m = -2, 0, 2$ mágneses kvantumszámú alterének rekonstruálására [9]. Módszerünk alapjául a disszipatív rendszerek kvantumállapotának preparálására bemutatott eljárás [5] szolgál. A kísérleti megvalósítás egyszerű: a rekonstruálni kívánt energiaszint nívóit koherens fényimpulzussal csatolni kell egy gerjesztett szint nívóihoz. A csatolás következtében a rendszer Rabi oszcillációkat végez a két szint között, s ez a folyamat addig tart, amíg a fényimpulzusok által definiált sötét altérbe nem pumpálódik a rendszer, miközben a populáció egy része elvész a további disszipációs csatornákon keresztül. A sötét altérben maradt populációt megmérve és a mérést különféle polarizációjú csatoló impulzusokra elvégezve egy inverziós formulával meg lehet kapni a rendszer kiindulási kvantumállapotát.

2. Kvantuminformatikai alkalmazások

Alapvető kvantumkapuk implementálása nanostruktúrákban

A félvezető nanostruktúrák – mesterséges atomok – számos előnnyel rendelkeznek az atomokkal szemben, ezért rengeteg javaslat születik kvantumbitként történő felhasználásukra. Az OTKA pályázat keretében több javaslatot tettünk ebben a témakörben.

A kidolgozott robusztus koherens kontroll sémák alapján Josephson átmeneten alapulú mágneses fluxus kvantumbitekre (SQUID) bemutattunk egy általános egy bites kvantumkaput, továbbá két kvantumbit összefonását eredményező művelet implementációját [10]. Az egy bites művelet alapja a királis molekulákban bemutatott forgatás, az összefonódott állapotot eredményező két bitesé pedig adiabatikus populáció transzfer a két SQUID között rádiófrekvenciás foton közvetítésével. Ugyanakkor kidolgoztunk egy kontrollált fázis-kaput két SQUID kvantumbit között [11]. A SQUID rendszerben bemutatott műveleteket kiterjesztettük kvantumpontokra (quantum dot) is [12, 13].

Kvantumhálózatok

A kvantuminformatikai alkalmazásokhoz kapcsolódóan megvizsgáltuk, hogy milyen mértékben lehet az összefonódottságot befolyásolni általában egy passzív elemekből álló kvantumoptikai hálózatban. Meghatároztuk a maximális elérhető kvantummechanikai összefonódottságot egy és két gerjesztés esetén Ising-típusú hálózatokban és eredményünket összevetettük a kvantumos gráfokra kimondott általánosabb tétellel. Vizsgáltuk továbbá, hogy milyen hatással van a zaj a véletlen bolyongásra, kétféle, koherens és inkoherens zajforrás esetén. Kimutattuk, hogy az átlagolt dinamikában bizonyos körülmények között exponenciális lokalizáció léphet fel [14]. A passzív kvantumoptikai hálózatok a kvantumos véletlen bolyongás

egy lehetséges megvalósítását adják. Két gerjesztés esetén azt találtuk, hogy a bolyongók találkozásának valószínűsége a klasszikustól alapvetően eltérően viselkedik, időben oszcillál, lecsengése gyorsabb mint a klasszikus esetben, de nem kvadratikusan gyorsabb [15].

Megvizsgáltuk, hogy két kvantumbit Hilbert terében mekkora lehet egy bázis elemeinek maximális összefonódottsága, ha a bázisnak van egy szeparálható eleme is. Megmutattuk, hogy bizonyos részlegesen összefonódott bázisokra vetítő mérések optimálisan használhatóak az összefonódottság mérés segítségével történő tisztításában. Ez a protokoll részlegesen összefonódott pár állapotokból bizonyos valószínűséggel erősebben összefonódott állapotokat állít elő [16].

Kisebb, 5-10 kvantumbites rendszerekben elemeztük a kvantummechanikai összefonódottság dinamikai viselkedését, a szokásos spin csatolások (Ising, Heisenberg, stb.) különböző topológiákban való alkalmazása esetén. Megmutattuk, hogy a kezdeti feltételek megfelelő beállításával kontrollálható a dinamikusan előálló kvantumállapotok összefonódottságának jellege. Rögzített csatolások segítségével, a kezdeti feltételtől függően elérhetünk a párösszefonódottság szempontjából optimális, illetve a sokrészű összefonódottság szempontjából optimális állapotokat. Megmutattuk, hogy ezek a tulajdonságok bizonyos értelemben egymás komplementerei. Megmutattuk, hogy mágneses tér alkalmazásával növelhető a bizonyos típusú összefonódottságok jelenlétének időtartama [17].

Kvantumbitek végtelen, egydimenziós láncának transzláció invariáns állapotai esetén nemtriviális kérdés a legközelebbi szomszéd kvantumbitek összefonódottsága. Numerikus optimalizációt végeztünk az úgynevezett végesen korrelált állapotok körében, amely alátámasztotta a párösszefonódottságnak az irodalomban sejtésként megfogalmazott maximális értékét. A végesen korrelált állapotok a lánc olyan kvantumállapotai ahol egy tetszőleges véges részrendszernek a többi kvantumbittel való korrelációit egy véges virtuális kvantumrendszerrel modellezhetjük. A formalizmus előnye hogy a végtelen rendszer kvantumállapotait egzaktul definiálja, és minden véges részrendszer kvantumállapota könnyen kiszámítható. Munkánkban erre alapozva részletesen elemeztük a párösszefonódottság szempontjából optimális állapotok tulajdonságait. Az alkalmazott módszer az ismert DMRG eljárásokkal szoros kapcsolatban áll, várhatóan más kvantummechanikai soktestprobléma megoldására is alkalmazható lesz [18].

A kvantumprocesszorok olyan rögzített kvantum logikai hálózatok, amelyek képesek egy kvantumbit regiszteren műveletek egy tág osztályát elvégezni, egy másik, úgynevezett programregiszter kvantumállapotától függően. Az ilyen elrendezések alkalmazását vizsgáltuk kvantumbitek markovi dekoherenciájának kontrollált szimulálására. Megmutattuk, hogy egy két programbites determinisztikus processzorral tetszőleges fáziscsillapító csatorna szimulálható [19].

Kvantumbitek viselkedését tanulmányozva kvantuminformatikai tisztítási protokollokban egy újfajta kaotikus dinamikát találtunk, amely eltér a szokásos kvantumkáosztól. Az iteratív dinamika egy nemlineáris, komplex leképezéshez vezet, ahol a nemunitér időfejlődést a mérésekkel való szelekció hozza létre. Sikerült bebizonyítani, hogy a kvantumállapotok átfedésével definiált Ljapunov exponens pozitív [20]. A kialakuló komplex káosz a tisztítási protokoll során is megjelenik, és a stabilitási tartományon kívül egy tranziens metastabil állapot után irreguláris viselkedés jelenhet meg [21].

Folytonos változós kvantuminformatika

A koherens állapotokkal definiált kvantumbit két, a fázistérben egymástól távol eső koherens állapot szuperpozíciója. Ennek dinamikáját vizsgáltuk veszteséges csatornában. A Bloch-gömb segítségével teljes képet adtunk az állapot torzulásáról a veszteség hatására. Megmutattuk, hogy ha a környezet összenyomott vákuum-állapotban van, az kedvezően hat a legsérülékenyebb ortogonális szuperpozíciók, – az ún. páros és páratlan koherens állapotok – megkülönböztethetőségére [22, 23].

Kiterjesztettük a véges dimenziós determinisztikus távoli állapot preparációs sémát (RSP, Remote State Preparation) folytonos változós kvantumrendszerekre [24]. Megmutattuk, hogy elvileg lehetséges olyan állapotok távoli előállítása, melyeket egy függvény paraméterez, miközben a klasszikus kommunikációs költség csak egy valós szám.

3. Jelenségek fáziskoherens közegekben

Fáziskoherens közegnek az olyan speciálisan preparált közeget nevezzük, ahol a közeget alkotó atomok két vagy több kvantumállapota koherens szuperponált állapotban van. Egy ilyen közegben a fényimpulzusok terjedése nem a szokványos módon történik a fellépő kvantuminterferencia jelenségek miatt. A [25] cikkben megmutattuk, hogy megfelelően választott helyfüggő atomi szuperponált állapot esetén 100% hatásfokú nemlineáris frekvenciakonverzió érhető el, szemben a konstans szuperpozíciójú fázsikoherens közegben kapható 50% hatásfokkal. Ebből az eredményből és korábbi, fáziskoheren közegekre vonatkozó eredményeinkből írtuk a [26] meghívott összefoglaló cikket.

A fáziskoheren közegek médiumként szolgálhatnak az általános relativitáselmélet optikai analógiáinak megvalósításához. A spontán párkeltéshez vezető helyzetek (Unruh-effektus, Hawking effektus) és az ezzel analóg, mozgó közegekben terjedő hullámoknál bekövetkező hullámkatasztrófák közös jellemzője a logaritmikus fázisszingularitás. Ez a viselkedés megjelenik egy sor jelenség modellezésénél, így többek között fényterjedés egy gravitációs fekete lyuk környékén, hangterjedés a lokális hangsebességet átlépő mozgó közegben, szinguláris dielektrikumban terjedő elektromágneses hullámok, illetve elektromágnesesen indukált átlátszóság körülményei között (fáziskoheren közeg) terjedő ún. lassú fény a csoportsebesség zéró pontja körül. Az ismert példák mindegyikében a logaritmikusan szinguláris fáziskitevő valós része egész vagy félegész szám. Általánosan, a Lagrange függvényből kiindulva sikerült belátnunk, hogy ez a tulajdonság, néhány alapvető feltétel teljesülése esetén mindig igaz. A fizikailag érdekes egyirányú illetve szimmetrikus esetekben a logaritmikusan szinguláris fáziskitevő valós része mindig egész vagy félegész szám [27].

A gravitációs fekete lyukak egyik legígéretesebb analóg modellje a lokális hangsebességet átlépve mozgó Bose-Einstein kondenzátum. Itt várható egyes modellek szerint, hogy a közegben terjedő hanghullámok a Hawking által megjósolt termikus sugárzást produkálják. A kísérleti megvalósítás azonban mindeddig még nem történt meg. Egy kvázi-egydimenziós áramlást alapul véve vizsgáltuk milyen feltételek között jöhet létre a lokális hangsebességet meghaladó áramlás. Kimutattuk, hogy Gauss-nyalábbal csapdázott kondenzátum esetén kettős eseményhorizont figzelhető meg. Megadtuk azt a kritikus minimális potenciált, amely konstans területű csapdázás esetén szükséges ahhoz, hogy az eseményhorizont megjelenjen. Kiszámítottuk az analóg Hawking-sugárzás hőmérsékletét és megmutattuk, hogy az csupán a csapdázó potenciál erősségétől függ [28].

Hivatkozások

[1] N.V. Vitanov, Z. Kis, and B.W. Shore
Coherent excitation of a degenerate two-level system by an elliptically polarized laser pulse
Phys. Rev. A 68, 063414/1-16 (2003).

[2] Z. Kis, A. Karpati, B.W. Shore, and N.V. Vitanov
Stimulated Raman adiabatic passage (STIRAP) among degenerate-level manifolds
Phys. Rev. A 70, 053405/1-20 (2004).

[3] Z. Kis, N.V. Vitanov, A. Karpapti, C. Barthel, K. Bergmann
Creation of arbitrary coherent superposition states by stimulated Raman adiabatic passage
Phys. Rev. A 72, 033403 (2005).

[4] Z. Kis, E. Paspalakis, F. Renzoni, and S. Stenholm
Controlling material by light and light by material via adiabatic processes
Acta Phys. Hun. B 20, 161-164 (2004).

[5] A. Karpati, Z. Kis, and P. Adam
Engineering mixed states in a degenerate four-state system
Phys. Rev. Lett. 93, 193003/1-4 (2004).

[6] I. Thanopulos, E. Paspalakis, and Z. Kis
Laser-driven coherent manipulation of molecular chirality
Chem. Phys. Lett. 390, 228-235 (2004).

[7] A. Karpati, P. Adam, Z. Kis, and J. Janszky
Stochastic unraveling of the time-evolution operator of open quantum system
Europhys. Lett. 75, 209 (2006).

[8] A. Karpati, P. Adam, J. Janszky
A method for calculating two-time correlation functions in the quantum trajectory approach
J. Opt B – Quant. Semicl. Opt. 6, S79-S83 (2004).

[9] C. Barthel, Z. Kis, U. Schneider, and K. Bergmann
Tomographic reconstruction of the quantum state in degenerate atomic systems
Phys. Rev A *submitted*

[10] Z. Kis and E. Paspalakis
Arbitrary rotation and entanglement of flux SQUID qubits
Phys. Rev. B 69, 024510/1-6 (2004).

[11] N. Sangouard, E. Paspalakis, Z. Kis, J. Janszky, and M. Fleischhauer
High fidelity logic gates for SQUID-qubits coupled to LC resonators
Phys. Rev. A *submitted*

[12] E. Paspalakis, Z. Kis, E. Voutsinas, A.F. Terzis
Controlled rotation in a double quantum dot structure
Phys. Rev. B 69, 155316/1-5 (2004).

[13] Z. Kis and E. Paspalakis
Controlled creation of entangled states of excitons in coupled quantum dots
J. Appl. Phys. 96, 3435-3439 (2004).

[14] J. Novotný, M. Štefaňák, T. Kiss, I. Jex:
Control of entanglement in Ising-type networks with one and two excitations
J. Phys. A – Math. Gen. 38, 9087-9103 (2005).

[15] M. Štefaňák, T. Kiss, I. Jex and B. Mohring
The meeting problem in the quantum walk
J. Phys. A – Math. Gen. 39, 14965-14983 (2006).

[16] M. Koniorczyk and V. Buzek
Nonmaximally entangled bases and their application in entanglement purification via swapping
Phys. Rev. A 71, 032331 (2005).

[17] M. Koniorczyk, P. Rapcan, and V. Buzek
Direct versus measurement-assisted bipartite entanglement in multiqubit systems and their dynamical generation in spin systems
Phys. Rev. A 72, 022321 (2005).

[18] M. Koniorczyk, V. Buzek, and P. Adam
Simulation of generators of Markovian dynamics on programmable quantum processors
Eur. Phys. J. D 37, 275-281 (2006).

[19] B. Hiesmayr, M. Koniorczyk, and H. Narnhofer
Maximizing nearest-neighbor entanglement in finitely correlated qubit chains
Phys. Rev. A 73, 032310 (2006).

[20] T. Kiss, I. Jex, G. Alber, and S. Vymětal
Complex chaos in the conditional dynamics of qubits
Phys. Rev. A 74, 040301R (2006).

[21] T. Kiss, I. Jex, G. Alber and S. Vymětal
Complex chaos in conditional qubit dynamics and purification
Acta Phys. Hung. B, accepted for publication.

[22] J. Asboth, P. Adam, M. Koniorczyk, and J. Janszky
Coherent-state qubits: entanglement and decoherence
Eur. Phys. J. D 30, 403-410 (2004).

[23] A. Gabris, P. Adam, M. Koniorczyk, and J. Janszky
Distuingishing Schroedinger cats in lossy environment
J. Opt. B – Quant. Semicl. Opt. 6, S84-S89 (2004).

[24] Z. Kurucz, P. Adam, Z. Kis, and J. Janszky
Continuous variable remote state preparation
Phys. Rev. A 72, 052315 (2005).

[25] Z. Kis and E. Paspalakis
Enhancing nonlinear frequency conversion using spatially dependent coherence
Phys. Rev. A 68, 043817/1-9 (2003).

[26] E. Paspalakis and Z. Kis
Novel Nonlinear Optical Response of Phase Coherent Media
Recent Res. Devel. Optics 3, 419-439 (2003) (invited).

[27] T. Kiss and U. Leonhardt
Towards a classification of wave catastrophes
J. Opt. A – Pure and Applied Optics 6, S246 - S247 (2004).

[28] S. Giovanazzi, C. Farrel, T. Kiss, U. Leonhardt:
Conditions for one-dimensional supersonic flow of quantum gases
Phys. Rev. A 70, 063602 (2004).

High fidelity logic gates for SQUID-qubits coupled to LC resonators

N. Sangouard,[1] E. Paspalakis,[2] Z. Kis,[1,3] J. Janszky,[3] and M. Fleischhauer[1]

[1] *Fachbereich Physik, Universtät Kaiserslautern, Erwin-Schroedinger Strasse, D-67663 Kaiserslautern, Germany*
[2] *Materials Science Department, School of Natural Sciences, University of Patras, Patras 265 04, Greece*
[3] *Research Institute for Solid State Physics and Optics, P.O. Box 49, H-1525 Budapest, Hungary*

(Dated: June 19, 2006)

We propose a scheme for high-fidelity quantum logic gates based on superconducting quantum interference devices (SQUID). The qubits are encoded in the two lowest (ground) states of an asymmetric SQUID. To realize single- and two-qubit quantum operations, the SQUIDs are coupled to external microwave fields as well as to a common high-Q quantized LC resonator in a tripod coupling scheme involving the two stable ground states, an additional lower level (auxiliary state), and an excited state. Due to the rather large dipole moments of SQUIDs, conditions equivalent to the strong coupling regime of cavity-QED can easily be reached. To accommodate the parameter uncertainties inherent to any solid-state system we propose a scheme based on adiabatic passage along quasi-dark states. Moreover, the proposed pulse sequence minimizes the occupation of the decaying auxiliary state, leading to high fidelity operations.

PACS numbers: 03.67.Lx, 85.25.Dq

In the past decade considerable effort has been devoted to the development of solid-state systems for realizing a scalable quantum computer. Josephson-junction based quantum bits (qubits) [1] are one of the most promising candidates to encode quantum information: Superconducting quantum interference devices (SQUIDs) possess very large dipole moments, several orders of magnitude larger than atomic systems, which provides strong coupling to electromagnetic fields. Moreover, Josephson-junction based qubits can be coupled in various ways using elements of microelectronics, e.g. capacitors and inductances [2–5]. In Refs. [4, 5] an LC circuit has been proposed for a quantum coupling of superconducting charge qubits. This coupling scheme has been applied for SQUIDs as well [6]. Here the LC circuit corresponds to a high-Q one-dimensional cavity with small effective mode volume. The large dipole moment of SQUIDs together with the small effective mode volume of the LC resonator make it comparatively easy to achieve the strong coupling regime, where the vacuum Rabi-frequency g of the resonator coupling is much larger than both the resonator decay rate κ and the decay rate γ of the involved transitions. In particular, in [4, 5], a value of $g^2/(\kappa\gamma) \approx 10^4$ was reported, which is two orders of magnitude larger [7] than achievable in cavity quantum electrodynamics (CQED) [8].

However, solid-state devices are artificially created objects, hence their characteristic properties are non-uniform. Transition frequencies, dipole moments etc. vary from sample to sample. A relevant quantum computation would require the usage on the order of 10^4 qubits, hence we need a control scheme which is tolerant with respect to the fluctuations of system parameters. Adiabatic methods fall into this category. Although there exists several proposals for the construction of one- and two-qubit logic gates [9–15] by adiabatic passage in atomic system, they all require the use of elementary systems which have in addition to the two (meta)stable qubit states an auxiliary third (meta)stable state, which is populated throughout the operation. In SQUIDs where the qubit states are encoded in the quantized flux states, there are, however, at most two (meta)stable, localized states, and even these states are subject to dephasing. Hence, for implementing quantum logic, schemes are needed which make a compromise between (*a*) short operation time to diminish the influence of decoherence and (*b*) adiabaticity required for robustness. In the present paper, we propose corresponding schemes adapted to SQUID configurations. In particular, we consider a swap gate and an entangling gate. Compared to alternative proposals [6, 12, 15–17], our scheme combines several advantages: A small number of pulses is used defining *simple algorithms*. Moreover, the control scheme is adiabatic, *hence it is tolerant to nonuniform device properties*, such as energy-level separation and magnitude of the dipole moments. As mentioned above, in SQUID systems the auxiliary state is necessarily an excited, decaying state unlike in atomic systems. Therefore, it is a particular advantage of our scheme that the auxiliary state is only briefly populated, hence *the effects of dissipation are greatly reduced*.

Let us consider a SQUID consisting of a micron sized superconducting loop interrupted by a Josephson junction. In this system, the magnetic flux Φ that intercepts the SQUID loop is subject to the potential [18]

$$U(\Phi) = \frac{(\Phi - \Phi_x)^2}{2L} - E_J \cos\left(2\pi \frac{\Phi}{\Phi_0}\right). \qquad (1)$$

Here, L is the SQUID inductance, Φ_x is the magnetic flux resulting from an external magnetic field, $E_J = I_c\Phi_0/2\pi$ is the maximum value of the Josephson energy, with I_c being the critical current of the junction, and $\Phi_0 = h/2e$

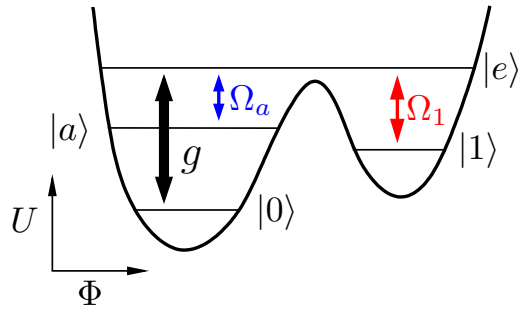

FIG. 1: (Color online) Coupling scheme for the SQUID system: Ω_a and Ω_1 describe the Rabi frequencies of classical external microwave fields, whereas g stand for the coupling strength between the SQUID and the LC circuit field.

is the flux quantum. We describe a realistic SQUID system [19] characterized by the inductance $L = 100$ pH, the capacitance $C = 40$ fF and the critical current I_c=3.95 μA. We also take $\Phi_x \approx \Phi_0/2$. For this set of parameters, the potential exhibits a double-well shape, see fig. 1, the energy levels are given by $E_0 = 0$, $E_1 = 0.08199\,\text{meV}$, $E_a = 0.18152\,\text{meV}$, and $E_e = 0.32073\,\text{meV}$. The two localized ground states form the qubit states $\{|0\rangle, |1\rangle\}$. It would be desirable to have at least three potential wells with three localized ground states. This would require either the increase of the Josephson energy, or the increase of the SQUID inductance. Both quantities are, however, limited by the physical properties of the junction, and it seems very difficult to obtain a triple-well potential. Thus any auxiliary state is always an excited state. Furthermore, although the SQUID states have comparatively long T_1 time, the dephasing time (T_2) is short thus requiring a short operation time.

We consider a four level tripod-type coupling configuration of such a rf-SQUID qubit (see fig. 1). The ground state $|0\rangle$ is coupled resonantly to an excited state $|e\rangle$ by the quantized field of a microwave circuit (of constant coupling g). The state $|1\rangle$ and the auxiliary state $|a\rangle$ are coupled to $|e\rangle$ by external microwave fields. These couplings are parameterized by the Rabi frequencies Ω_ℓ, the subscript index $\ell = 1, a$ refers to the coupled state. The LC coupling strength and the Rabi frequency associated with the microwave field read [17]

$$g = \frac{1}{L}\sqrt{\frac{\omega_c}{2\mu_0\hbar}}\langle 0|\Phi|e\rangle \int_S \boldsymbol{B}_c(\boldsymbol{r})\, d\boldsymbol{S}\,, \tag{2a}$$

$$\Omega_\ell = \frac{1}{2L\hbar}\langle \ell|\Phi|e\rangle \int_S \boldsymbol{B}_{\rm mw}(\boldsymbol{r})\, d\boldsymbol{S}\,, \tag{2b}$$

where S is the surface covered by the SQUID loop, $\boldsymbol{B}_q(\boldsymbol{r})$ ($q = c, \text{mw}$) is the magnetic field intercepting the SQUID, and $\langle \ell|\Phi|\jmath\rangle$ are effective dipole matrix elements in the generalized coordinates. For realizing quantum logic we need several such qubits, placed into a cavity and individually addressable. The individual addressing can be achieved by wires placed close to the SQUID rings [20]. Single qubit operations can be implemented by coupling the qubit states of a single SQUID in a lambda-type configuration [21, 22]. These are local operations, each qubit state being manipulated independently. Combining the single-qubit gates with any two-qubit gate provides a universal set [23], from which an arbitrary quantum circuit can be built.

Now we turn our attention to the robust implementation of a controlled-phase (Cphase) gate. Among the qubits belonging to the register, we chose two SQUIDs corresponding to the control and target qubits, respectively. We assume that the cavity coupling is not resonant with the other qubits. This could be achieved, e.g. by switching on local off-resonant couplings Ω_a to induce a Stark shift S of the excited states $|e\rangle$ such that $g/S \ll 1$. The RWA Hamiltonian of the Cphase gate operation is given in the rotating frame by

$$\begin{aligned} H \;=\; & \hbar\Delta(|e,c\rangle\langle e,c| + |e,t\rangle\langle e,t|) + \\ & \frac{\hbar}{2}\Big(\Omega_1^{(c)}|e,c\rangle\langle 1,c| + g^{(c)}|e,c\rangle\langle 0,c|\, b \\ & + \Omega_a^{(t)}|e,t\rangle\langle a,t| + g^{(t)}|e,t\rangle\langle 0,t|\, b + \text{h.c.}\Big)\,, \end{aligned} \tag{3}$$

where b ($b^\dagger$) is the annihilation (creation) operator of the LC oscillator. The one-photon detuning Δ is defined as $\Delta = (E_e - E_1)/\hbar - \omega_{1,\text{mw}}$, and two photon resonance is assumed for the microwave and cavity photons, $(E_1 - E_0)/\hbar = \omega_c - \omega_{1,\text{mw}}$, as well as for the two microwave photons $(E_a - E_1)/\hbar = \omega_{1,\text{mw}} - \omega_{a,\text{mw}}$. Here, E_i ($i = 0, 1, a, e$) are the eigenenergies associated with the SQUID qubit states $|i\rangle$. The superscripts (t, c) refer to the control or target qubits, respectively. The initial state of the two-qubit subsystem is given by

$$|\psi_0\rangle = \Big(c_{00}|00\rangle + c_{01}|01\rangle + c_{10}|10\rangle + c_{11}|11\rangle\Big)|0\rangle\,, \tag{4}$$

where the first digit denotes the state of the control qubit, the second one corresponds to the target qubit and the state $|0\rangle$ at the end describes the photon vacuum, i.e. an empty cavity. The Cphase gate operation consists of two steps:

Step 1: transfer the population from state $|10\rangle|0\rangle$ to state $|0a\rangle|0\rangle$ via the LC resonator mode, without altering the populations in the states $|00\rangle|0\rangle$, $|01\rangle|0\rangle$ and $|11\rangle|0\rangle$ by an adiabatic process. The Hamiltonian of Eq. (3) admits the following dark states [9, 12, 15, 22] (apart from normalization factors):

$$|00\rangle|0\rangle, \tag{5a}$$

$$|01\rangle|0\rangle, \tag{5b}$$

$$g^{(c)}\Omega_a^{(t)}|10\rangle|0\rangle + g^{(t)}\Omega_1^{(c)}|0a\rangle|0\rangle - \Omega_1^{(c)}\Omega_a^{(t)}|00\rangle|1\rangle, \tag{5c}$$

$$\Omega_1^{(c)}|01\rangle|1\rangle - g^{(c)}|11\rangle|0\rangle\,. \tag{5d}$$

For the population transfer we use the third dark state (5c). The applied pulse sequence is the counterintuitive

pulse sequence of STIRAP [24], i.e. $\Omega_a^{(t)}$ applied before $\Omega_1^{(c)}$ with some overlap. Unlike in the original proposal [9], here we allow for $g \approx \Omega_{\max}$, $\Omega_{\max} = \max\{\Omega_a^{(t)}, \Omega_1^{(c)}\}$. This is done in order to make the population transfer faster, such that the main source of decoherence, which is the decay of the auxiliary state, is reduced (see later discussion). The drawback is that now the LC resonator attains a finite population during the operation time. It can be readily seen that the first two states in the superposition state of Eq. (4) are not involved in the population transfer, since they coincide with the dark states (5a) and (5b), respectively. The fourth state in $|\psi_0\rangle$ coincides with the dark state of Eq. (5d) at the beginning of the population transfer. Then, some population is placed to the state $|01\rangle|1\rangle$, and at the end of the pulse sequence the population returns to state $|11\rangle|0\rangle$. The resulting state is

$$|\psi_1\rangle = \Big(c_{00}|00\rangle + c_{01}|01\rangle + e^{\imath(\varphi_a^{(t)} - \varphi_1^{(c)})} c_{10}|0a\rangle + c_{11}|11\rangle\Big)|0\rangle\,,$$

where $\varphi_a^{(t)} - \varphi_1^{(c)}$ is the relative phase of the laser fields $\Omega_1^{(c)}$ and $\Omega_a^{(t)}$.

Step 2: repeat the previous population transfer process with reversed pulse order, i.e. $\Omega_1^{(c)}$ followed by $\Omega_a^{(t)}$, and allowing some phase shift $(\varphi_a^{(t)} - \varphi_a'^{(t)})$ for $\Omega_a^{(t)}$. This process yields the state

$$|\psi_2\rangle = \Big(c_{00}|00\rangle + c_{01}|01\rangle + e^{\imath(\varphi_a^{(t)} - \varphi_a'^{(t)})} c_{10}|10\rangle + c_{11}|11\rangle\Big)|0\rangle$$

which coincides with the output state of a Cphase gate. The phase is set by the relative phase of the laser pulses applied in the $1st$ and $2nd$ steps and can be controlled with high accuracy. Hence, we avoid the use of non-robust dynamical phases, which depend on the area of the applied pulses [10, 12, 25–27]. Furthermore, since the second pulse of the $1st$ step and the first pulse of the $2nd$ step are the same, the entangling gate can be realized with a simple sequence of three pulses. Most importantly the auxiliary state is only populated when the intermediate pulse $\Omega_1^{(c)}$ is larger than $\Omega_a^{(t)}$.

The exchange of unknown quantum information between two qubits can be realized by a SWAP gate. The SWAP operation could be decomposed to three Cphase gate and nine one-qubit gates [15]. We show in what follows a simpler alternative technique which uses an additional qubit. The RWA Hamiltonian of the SWAP operation is given in the rotating-wave picture by

$$\begin{aligned} H \;=\; & \hbar\Delta(|e,x\rangle\langle e,x| + |e,y\rangle\langle e,y| + |e,a\rangle\langle e,a|) \\ & + \frac{\hbar}{2}\Big(\Omega_1^{(x)}|e,x\rangle\langle 1,x| + g^{(x)}|e,x\rangle\langle 0,x|\,b \\ & + \Omega_1^{(y)}|e,y\rangle\langle 1,y| + g^{(y)}|e,y\rangle\langle 0,y|\,b + \\ & + \Omega_1^{(a)}|e,a\rangle\langle 1,a| + g^{(a)}|e,a\rangle\langle 0,a|\,b + \text{h.c.}\Big)\,. \end{aligned} \quad (6)$$

Besides coupling to the cavity field, the two SQUID sites x, y and the ancilla qubits interact with an external microwave field $\Omega^{(q)}$ $(q = x, y, a)$ nearly resonant with the transition $|1,q\rangle$–$|e,q\rangle$. The initial state of the three-qubit subsystem is given by

$$|\psi_0\rangle = |0\rangle(c_{00}|00\rangle + c_{01}|01\rangle + c_{10}|10\rangle + c_{11}|11\rangle)|0\rangle\,, \quad (7)$$

where the first digit denotes the state of the ancilla qubit prepared in state $|0\rangle$, the second and third ones refer to the two sites x and y, respectively, and at the end $|0\rangle$ describes the photon number in the cavity. The SWAP operation consists of three steps similar to the Cphase operation:

Step 1: transfer the population from state $|0_a 1_x\rangle|0\rangle$ to state $|1_a 0_x\rangle|0\rangle$ using the pulse-sequence $\Omega_1^{(a)}$–$\Omega_1^{(x)}$ by the adiabatic following of the dark state

$$\begin{aligned} & g^{(a)}\Omega_1^{(x)}|1_a 0_x\rangle|0\rangle + g^{(x)}\Omega_1^{(a)}|0_a 1_x\rangle|0\rangle \\ & \quad -\Omega_1^{(a)}\Omega_1^{(x)}|0_a 0_x\rangle|1\rangle. \end{aligned} \quad (8)$$

The state $|0_a 0_x\rangle|0\rangle$ is a dark state, therefore, the populations in the first two states of the initial superposition state of Eq. (7) are preserved. The resulting state is

$$|\psi_1\rangle = (c_{00}|0\rangle|00\rangle + c_{01}|0\rangle|01\rangle + c_{10}|1\rangle|00\rangle + c_{11}|1\rangle|01\rangle)|0\rangle\,.$$

Step 2: transfer the population from state $|0_x 1_y\rangle|0\rangle$ to state $|1_x 0_y\rangle|0\rangle$ using the pulse-sequence $\Omega_1^{(x)}$–$\Omega_1^{(y)}$. This population transfer is realized by the adiabatic following of the dark state (8) where the superscript indices (a) and (x) have to be replaced by (x) and (y), respectively. This transfer leads to the state

$$|\psi_2\rangle = (c_{00}|0\rangle|00\rangle + c_{01}|0\rangle|10\rangle + c_{10}|1\rangle|00\rangle + c_{11}|1\rangle|10\rangle)|0\rangle\,.$$

Step 3: transfer the population from state $|1_a 0_y\rangle|0\rangle$ to state $|0_a 1_y\rangle|0\rangle$ using the pulse-sequence $\Omega_1^{(y)}$–$\Omega_1^{(a)}$. During the transfer, the system follows the dark states of Eq. (8) where the indices (a) and (x) should be replaced by (y) and (a), respectively. The resulting state coincides with the output state of the SWAP gate

$$|\psi_3\rangle = (c_{00}|0\rangle|00\rangle + c_{01}|0\rangle|10\rangle + c_{10}|0\rangle|01\rangle + c_{11}|0\rangle|11\rangle)|0\rangle\,.$$

Since the second pulse of each step is again the same as the first one of the next step, the SWAP gate can be implemented by using four pulses only. Similarly to the Cphase gate, the resonator is negligibly populated provided that the resonator coupling is significantly stronger than the microwave field couplings. It is worth noting that as opposed to the Cphase gate the excited SQUID states are never populated during the process. This leads to a higher fidelity of the SWAP gate as compared to the Cphase gate.

In order to verify our scheme and to estimate the fidelity of the gate operations we compared the result of

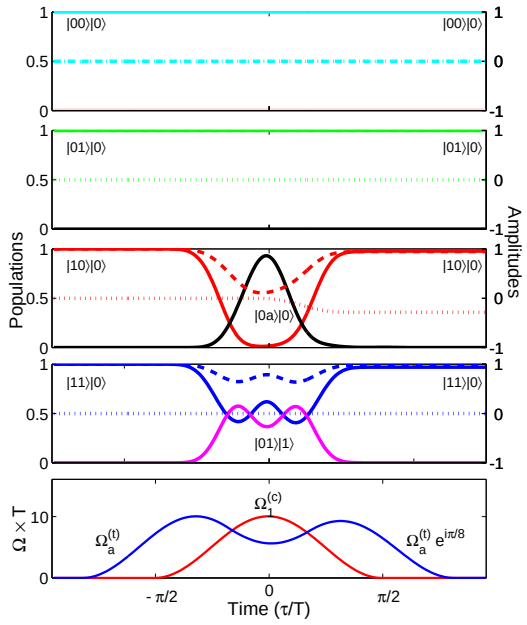

FIG. 2: (Color online) Numerical simulation of a Cphase($-\pi/8$) gate. Populations (full line and left scale) and probability amplitudes (real part dashed line, imaginary part dotted line on the right scale) versus time for the initial states (from the top to the bottom) $|00\rangle|0\rangle$, $|01\rangle|0\rangle$, $|10\rangle|0\rangle$, $|11\rangle|0\rangle$. Last frame: Rabi frequencies as a function of time.

the analytic consideration with numerical simulations for the Cphase($-\pi/8$) gate, see fig. 2. The time evolution of four states is shown: the states $|00\rangle|0\rangle$, $|01\rangle|0\rangle$ and $|11\rangle|0\rangle$ are unchanged after the interaction with the three subsequent pulses, whereas $|01\rangle|0\rangle$ acquires a phase shift of $-\pi/8$. The sequence of pulses is induced by cosine squared pulses and the corresponding Rabi frequencies are given by $\Omega_a^{(t,1)}(\tau) = \Omega_1^{(c)}(\tau + T)$, $\Omega_a^{(t,2)}(\tau) = \Omega_1^{(c)}(\tau - T)$, $\Omega_1^{(c)}(\tau) = \Omega_{\max} \cos(\tau/T)^2$. In order to fulfill adiabaticity, the conditions $\Omega_{\max} T, g\,T \gg 1$ has to be satisfied. We chose pulse durations in the nanosecond regime $T \approx 15\,\mathrm{ns}$. In Ref. [28, 29] the measured energy relaxation time for a Nb flux qubit was a few tens of μs, and the dephasing time of several tens of ns. In Ref. [30], even a dephasing time of a few μs has been observed in three-Josephson-junction flux qubits. We thus assume that both relaxation and dephasing processes do not play a role in the dynamics on the timescale of the proposed gate operations. Thus the main source of error is now the resonator decay. We describe a realistic SQUID system and use the parameters of Refs. [4, 7, 19], i.e. $\Omega_{\max}/2 \approx g/2 \approx 3.1 \times 10^8 \mathrm{s}^{-1}$ such that $\Omega_{\max} T = gT = 10$. Since for these specific values the cavity coupling is not stronger than the microwave field coupling, we study the sensitivity of the proposed gates with respect to dissipation of the resonator. We include into the model realistic cavity decay chosen to be $\kappa \approx 1.3 \times 10^6\ \mathrm{s}^{-1}$ [7]. Depending on the initial state, the fidelity $|\langle\psi_f(\text{with losses})|\psi_f(\text{without losses})\rangle|$ of the Cphase($-\pi/8$) gate varies between 97% and 100%. The average fidelity coefficient calculated for c_{00}=c_{01}=c_{10}=c_{11}=$1/\sqrt{4}$ is 98.5%.

In summary, in this work we have presented simple, efficient and robust schemes, based on adiabatic methods, for the implementation of high fidelity logic operations. The schemes rely on state of the art technologies and thus offers promising perspectives to implement quantum computation and quantum information processing in solid state systems in the near future.

The authors thank A. Lupascu for fruitful discussions. This work has been supported by the EU Research and Training network QUACS. NS acknowledges La Fondation Carnot for financial support. JJ and ZK acknowledge the support of the Research Fund of the Hungarian Academy of Sciences under contracts T043287 and T049234. ZK acknowledges the support of the EU Transfer of Knowledge project CAMEL.

[1] Y. Makhlin, G. Schön and A. Shnirman, Rev. Mod. Phys. **73**, 357 (2001).
[2] A. Blais, A.M. van den Brink, and A.M. Zagoskin, Phys. Rev. Lett. **90**, 127901 (2003).
[3] F. Plastina, G. Falci, Phys. Rev. B **67**, 224514 (2003).
[4] A. Blais, R.S. Huang, A. Wallraff, S.M. Girvin, and R.J. Schoelkopf, Phys. Rev. A **69**, 062320 (2004).
[5] A. Wallraff, D.I. Schuster, A. Blais, L. Frunzio, R.-S. Huang, J. Mayer, S. Kumar, S.M. Girvin, R.J. Schoelkopf, Nature **431**, 162 (2004).
[6] C.P. Yang, S. Han, Phys. Rev. A **72**, 032311 (2005).
[7] C.P. Yang, Shih-I. Chu, and S. Han, Phys. Rev. Lett. **92**, 117902 (2004).
[8] J. McKeever, A. Boca, A.D. Boozer, J.R. Buck, and H.J. Kimble, Nature **425**, 268 (2003).
[9] T. Pellizzari, S.A. Gardiner, J.I. Cirac and P. Zoller, Phys. Rev. Lett. **75**, 3788 (1995).
[10] Z. Kis, and F. Renzoni, Phys. Rev. A **65**, 032318 (2002).
[11] F. Troiani, E. Molinari, U. Hohenester, Phys. Rev. Lett. 90, 206802 (2003).
[12] H. Goto and K. Ichimura, Phys. Rev. A **70**, 012305 (2004).
[13] C.P. Yang, Shih-I. Chu, and S. Han, Phys. Rev. A **70**, 044303 (2004).
[14] K. Roszak, A. Grodecka, P. Machnikowski, and T. Kuhn, Phys. Rev. B 71, 195333 (2005).
[15] N. Sangouard, X. Lacour, S. Guérin, H. R. Jauslin, Phys. Rev. A **72**, 062309 (2005).
[16] C.-P. Yang, S.-I Chu, and S. Han, Phys. Rev. A **70**, 044303 (2004).
[17] C.P. Yang, Shih-I. Chu, and S. Han, Phys. Rev. A **67**, 042311 (2003).
[18] J.R. Friedman, V. Patel, W. Chen, S.K. Tolpygo, and J.E. Lukens, Nature **406**, 43 (2000).
[19] E. Paspalakis and N.J. Kylstra, J. Mod. Optics **51** 1679 (2004).
[20] J.E. Mooij, T.P. Orlando, L. Levitov, Lin Tian, C.H. van der Wal, and S. Lloyd, Science **285**, 1036 (1999).

[21] Z. Zhou, Shih-I. Chu and S. Han, Phys. Rev. B **66**, 054527 (2002).
[22] Z. Kis and E. Paspalakis, Phys. Rev. B **69**, 024510 (2004).
[23] M.J. Bremner, C.M. Dawson, J.L. Dodd, A. Gilchrist, A.W. Harrow, D. Mortimer, M.A. Nielsen, T.J. Osborne, Phys. Rev. Lett. **89**, 247902 (2002).
[24] N.V. Vitanov, M. Fleischauer, B.W. Shore and K. Bergmann, Adv. At. Mol. Opt. Phys. **46**, 55 (2001).
[25] R.G. Unanyan, B.W. Shore, and K. Bergmann, Phys. Rev. A **59**, 2910 (1999).
[26] L.M. Duan, J.I. Cirac, and P. Zoller, Science **292**, 1695 (2001).
[27] R.G. Unanyan and M. Fleischhauer, Phys. Rev. A **69**, 050302(R) (2004).
[28] Y. Yu, D. Nakada, J.C. Lee, B. Singh, D.S. Crankshaw, T.P. Orlando, K.K. Berggren, and W.D. Oliver, Phys. Rev. Lett. **92**, 117904 (2004).
[29] W.D. Oliver, Y. Yu, J.C. Lee, K.K. Berggren, L.S. Levitov, and T.P. Orlando Science **310**, 1653 2005.
[30] E. Il'ichev, N. Oukhanski, A. Izmalkov, Th. Wagner, M. Grajcar, H.-G. Meyer, A. Yu. Smirnov, Alec Maasen van den Brink, M.H.S. Amin, and A.M. Zagoskin, Phys. Rev. Lett. **91**, 097906 (2003).

Tomographic reconstruction of the quantum state in degenerate atomic systems

C. Barthel,[1] Z. Kis,[1,2] U. Schneider,[3] and K. Bergmann[1]

[1] *Fachbereich Physik der Universität Kaiserslautern, 67653 Kaiserslautern,Germany*
[2] *H.A.S. Research Institute for Solid State Physics and Optics, H-1525 Budapest, P.O.Box 49, Hungary**
[3] *Institute für Physik, Johannes Gutenberg-Universität, 55099 Mainz,Germany*

(Dated: September 15, 2006)

A quantum state reconstruction procedure is proposed for retrieving the quantum state of a degenerate multistate system, in partical the quantum states in Zeeman manifolds. The scheme is based on a coherent pumping technique, in which the initial state space is coupled to excited states with an elliptically polarized laser pulse: due to spontaneous emission the system relaxes into the dark states defined by the filter laser and into some other states outside the initial state space. The population pumped into the dark subspace is measured in a subsequent step. It is shown that by varying the polarization state of the filter laser, the initial quantum state of the system can be retrieved from the measured populations with high fidelity. Finally, the accuracy of the state reconstruction procedure is studied.

PACS numbers: 03.65.Wj,32.80.Qk,32.80.Bx

I. INTRODUCTION

What are the relative phases in the superposition quantum state? This question is often asked when coherent light-matter processes are studied. The advent of high intensity, narrow bandwidth and coherent electromagnetic radiation sources (masers and lasers) opened several new research areas where atomic coherent superposition states play a central role. Nowadays such superpositions are routinely created in many laboratories, and a vast arsenal of phenomena is based on them. Just to mention but a few, preparation of Rydberg atoms [1, 2] and cavity QED experiments [3], coherent control of molecular dynamics [4], dark resonances and high precision spectroscopy [5], field propagation in phase coherent media [6, 7], and coherent control of atomic states [8–10].

The coherent superposition of nondegenerate states leads to the formation of wave packets, which are objects evolving with time. In this work we consider the coherent superposition of degenerate states, which are stationary objects with no dynamical phase involved. The Zeeman multiplets of levels with $J > 0$ provide such sets of degenerate levels. Spectroscopic measurements revealed first the occurrence of Zeeman coherences [5, 11–14]. Following these observations several applications have been developed that rely on Zeeman coherences. Examles are the Hanle effect [15–17], mapping of Zeeman coherences to cavity field [18–20], lasing without inversion [21–23], electromagnetically induced transparency [7, 24], slow down and storage of light pulses [25–27], coherent frequency conversion [28–30].

Superpositions of Zeeman sublevels can also be created systematically by means of π-pulse techniques [31, 32], or using the stimulated Raman adiabatic passage method [33–44]. All of the above cited methods are capable to various extents to control not only the modulus of the probability amplitudes associated with the components of the prepared superposition states, but the relative phases among them as well.

The preparation of such coherences is only part of the challenge. Equally challenging is the design of methods which allow the full characterization of such quantm states. We need a procedure that permits the evaluation of the complex probability amplitudes that define the superposition. Numerous proposals have been advanced for this purpose: holographic reconstruction schemes have been developed for Rydberg states [2, 45], the vibrational wave packet of diatomic molecules can be reconstructed by means of observing the time-gated fluorescence signal [46, 47], or using a holographic technique similar to the Rydberg atoms [48]. In case of Zeeman coherences, a projective reconstruction technique has been proposed [49, 50] and demonstrated experimentally [51]. In these last proposals, the Zeeman sublevels, on which the superposition state is prepared, are coupled to an excited degenerate level (an other Zeeman multiplet) by an elliptically polarized laser pulse, and part of the population is transferred to the excited states. By measuring the total population of the excited states [49–51], information can be inferred about not only the populations of the initial superposition state, but also about the coherences among the Zeeman sublevels as well. Repeating the projective measurement for various laser polarizations, the full set of parameters characterizing the superposition state can be retrieved from the measured populations. The advantage of this method is that in principle it can be applied to Zeeman multiplets with arbitrary number of components. The disadvantage is that it requires π-pulses, which are delicate to generate at optical frequency.

In the present paper we propose a method for reconstructing the superposition state on the $M = -2, 0, 2$ Zeeman sublevels of a $J = 2$ angular momentum state. Here J refers to the total angular momentum of the state, i.e. the sum of the orbital, spin and nuclear angular mo-

*Electronic address: zsolt@szfki.hu

mentums. Examples to systems to which our method can be applied are e.g. the $^3P_2$ level of the metastable neon, or the $F = 2$ levels of the alkali atoms, such as the widely used ^{23}Na, ^{85}Rb, ^{87}Rb, and ^{133}Cs. The reconstruction scheme is based on the coherent pumping technique of ref. [52]. The coherent pumping is realized by coupling the initial level manifold to an excited level manifold by an elliptically polarized laser pulse. The excitation process leads to the pumping part of the system into the dark states defined by the coherent coupling field. By repeating the pumping process several times with different laser polarizations one can steer the density matrix of the system to a required pure or mixed quantum state. In the proposed reconstruction scheme this coherent pumping technique is used to transfer part of the population from the initial state to the dark states of the system. The population in the dark states is measured in a subsequent step, allowing retrival of the parameters of the superposition state composed from the $M = -2, 0, 2$ manifold. This measurement scheme works in atomic beam experiments where a continuous stream of identically prepared paricles is available. Application of the scheme to trapped atoms requires many cycles of identical preparation followed by a measurement.

The paper is organized as follows: In the next section, Sec. II, the model system is presented and the master equation describing the measurement procedure is given. In Sec. III the late time solution of the master equation is determined. To this end, the left- and right-hand-side eigenstates belonging to eigenvalue zero of the Liouvillian are calculated. In Sec. IV, the reconstruction scheme is worked out for exciting pulses with rectangular envelope, because in this case some important relations can be obtained in a closed, algebraic form. Then in Sec. V the accuracy of the reconstruction procedure is analyzed with respect to the choice of the exciting laser polarization and phase, Sec. V A; to the use of pulses with Gaussian envelope instead of rectangular, Sec. V B; to the imperfect setting of the laser field polarization and phase, Sec. V C. We summarize the results and conclude the paper in Sec. VI.

II. THE MODEL SYSTEM

Qualitatively, our state-reconstruction procedure works as follows: the quantum state to be reconstructed is prepared within the Zeeman sublevels $M_g = -2, 0, 2$ of some ground state of the system, i.e. a stable or metastable state with total angular momentum of $J_g = 2$. The subspace spanned by these states is called initial state space. The reason of the restriction on the initial state space will be discussed at the end of Sec. IV. As part of the reconstruction process, all sublevels of the $J_g = 2$ level are coupled to the sublevels of an excited state with $J_e = 1$ by the so called filter laser: a coherent laser field with $\sigma^{\pm}$ polarization components. The state space can be divided into two coupled subspaces:

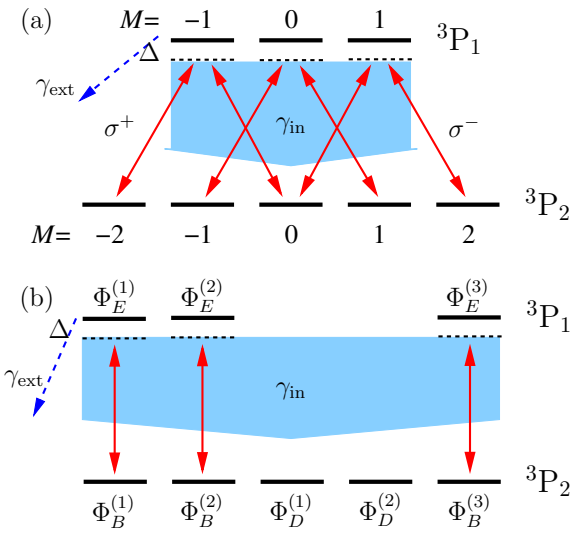

FIG. 1: Top (a): the level structure of metastable neon used in the state reconstruction procedure: The state space is spanned by the magnetic sublevels of the ^{3}P$_2$ level. These states are coupled to the magnetic sublevels of the ^{3}P$_1$ level with a nearly resonant, coherent laser pulse. Bottom (b): the coupling scheme in panel (a) in the dark-bright basis. The dark states are decoupled from the driving light pulses, however, they are populated through the spontaneous decay from the excited sublevels.

a smaller one which consists of the states $M_g = -1, 1$ of the ground level and of the state $M_e = 0$ of the excited level; a larger one consisting of the states $M_g = -2, 0, 2$ of the ground level (i.e. the states of the initial state space) and of the states $M_e = -1, 1$ of the excited level.

The coupling configuration is shown in Fig. 1 (a). The smaller and larger coherently coupled systems are not coupled by the filter laser, but they are coupled through the spontaneous decay from the excited level. The result of the excitation process can be easily understood in the dark-bright basis [5], defined by the filter laser: the dark states are decoupled from the driving laser pulses whereas the bright states, being coupled to excited states, undergo coherent oscillations.

In the dark-bright basis the system separates to a set of three two-state systems and two decoupled states [53] as shown in Fig. 1 (b). The excited states are decaying, hence the coherent oscillations are accompanied by spontaneous decay to lower laying states: the ground state sublevels under consideration and others outside of the ground state, e.g. in metastable neon the $^3P_1$ and $^1P_1$ levels which decay further to the electronic ground state $^1S_0$ of Neon. We call the former events "internal" and the latter "external". In the course of the internal decay process, both the bright and the dark states may get populated. However, the population in the dark states is

not redistributed in the course of the coherent excitation process. These populations can only increase due to the spontaneous decay from the excited level. The process continues until all population is removed from the bright subspace. As a result, some population is pumped into the dark subspace via the internal decay process, while the remaining population is pumped out of the ground level due to the external decay.

The fraction of the population remaining in the dark subspace depends on the initial state to be reconstructed, on the polarization and strength of the filter field, and on the magnitude of the internal and external decay rates. The population left in the dark subspace can be measured in a subsequent step [51]. This is a phase sensitive measurement, because the dark and bright states are defined by the σ_+ and σ_- components of the filter laser with controllable relative amplitude and phase. Therefore, by varying the polarization of the filter laser field one may infer information about the initial state of the system via population measurements.

In the following derivation we determine quantitatively the amount of population left in the dark subspace and provide a recipe how to adjust the polarization of the filter laser field in order to fully reconstruct the initial state of the systems.

The non-unitary dynamics outlined above is well described by the master equation

$$\begin{aligned}\frac{d}{dt}\varrho &= -\frac{\imath}{\hbar}[H,\varrho] - \frac{\gamma_{\rm ext}}{2}(L_e\varrho + \varrho L_e) + \\ &\quad \frac{\gamma_{\rm in}}{2}\sum_l \left(2L_l\,\varrho\,L_l^\dagger - L_l^\dagger L_l\,\varrho - \varrho\,L_l^\dagger L_l\right).\end{aligned} \tag{1}$$

The Hamiltonian part characterises the coherent interaction between the atom and the filter laser: in the RWA picture using the RWA approximation it reads

$$\boldsymbol{H} = \hbar \begin{array}{c} \\ e \\ g \end{array} \begin{array}{c} \begin{array}{cc} e & g \end{array} \\ \begin{bmatrix} \boldsymbol{\Delta} & \frac{1}{2}\boldsymbol{\Omega} \\ \frac{1}{2}\boldsymbol{\Omega}^\dagger & \mathbf{0} \end{bmatrix} \end{array}, \tag{2}$$

where the labels e and g indicate the structure of the Hamiltonian: g corresponds to the ground energy level, while e denotes the excited energy level. Here $\boldsymbol{\Delta}$ is a 3×3 diagonal matrix (with Δ in the diagonal and zero otherwise) that describes the detuning of the coupling fields from the transition frequency between the ground and excited levels, and the coupling matrix $\boldsymbol{\Omega}$ is defined as

$$\boldsymbol{\Omega} = \begin{bmatrix} \frac{\sqrt{6}}{\sqrt{10}}\Omega_+ & 0 & \frac{1}{\sqrt{10}}\Omega_- & 0 & 0 \\ 0 & \frac{\sqrt{3}}{\sqrt{10}}\Omega_+ & 0 & \frac{\sqrt{3}}{\sqrt{10}}\Omega_- & 0 \\ 0 & 0 & \frac{1}{\sqrt{10}}\Omega_+ & 0 & \frac{\sqrt{6}}{\sqrt{10}}\Omega_- \end{bmatrix} \tag{3}$$

where the amplitudes $\Omega_\pm$ are associated with the $\sigma_\pm$ polarization components of the driving field [54], see fig. 1. The Rabi frequencies are given by the amplitudes $\Omega_\pm$ multiplied by the Clebsch-Gordan coefficients (which are the square-root rational fractions in the $\boldsymbol{\Omega}$ matrix) associated with the dipole transitions between the $J_g = 2$ and $J_e = 1$ angular momentum states. In the coupling matrix the column index runs over the interval $[-2,\ldots,2]$ corresponding to the magnetic sublevels of the ground level, while the row index runs over the interval $[-1,0,1]$ corresponding to the magnetic sublevels of the excited level. In the master equation (1) the symbols $\gamma_{\rm in}$ and $\gamma_{\rm ext}$ characterise the internal and external radiative decay rates, respectively. The flip operators are defined as

$$\begin{aligned} L_- &= \frac{1}{\sqrt{10}}|g,0\rangle\langle e,-1| + \frac{\sqrt{3}}{\sqrt{10}}|g,+1\rangle\langle e,0| \\ &+ \frac{\sqrt{6}}{\sqrt{10}}|g,+2\rangle\langle e,+1|\,, \end{aligned} \tag{4a}$$

$$\begin{aligned} L_\pi &= \frac{\sqrt{3}}{\sqrt{10}}|g,-1\rangle\langle e,-1| + \frac{2}{\sqrt{10}}|g,0\rangle\langle e,0| \\ &+ \frac{\sqrt{3}}{\sqrt{10}}|g,+1\rangle\langle e,+1|\,, \end{aligned} \tag{4b}$$

$$\begin{aligned} L_+ &= \frac{\sqrt{6}}{\sqrt{10}}|g,-2\rangle\langle e,-1| + \frac{\sqrt{3}}{\sqrt{10}}|g,-1\rangle\langle e,0| \\ &+ \frac{1}{\sqrt{10}}|g,0\rangle\langle e,+1|\,, \end{aligned} \tag{4c}$$

where the subscript $l = -,\pi,+$ of L_l describes the change of the magnetic quantum number in the course of the transition. The states $|q,M\rangle$ correspond to the Zeeman sublevels of the ground or excited levels ($q = g,e$), where the index M refers to the magnetic quantum number of the sublevel. Finally, the projector L_e is defined by

$$L_e = \sum_{M=-1,0,+1} |e,M\rangle\langle e,M|\,. \tag{5}$$

It can be readily verified that

$$\sum_l L_l^\dagger L_l = L_e\,. \tag{6}$$

Therefore, the master equation (1) reads in a compact form

$$\begin{aligned}\frac{d}{dt}\varrho &= \mathcal{L}\,\varrho = -\frac{\imath}{\hbar}[H,\varrho] - \frac{\gamma_{\rm ext}+\gamma_{\rm in}}{2}(L_e\varrho + \varrho L_e) \\ &\quad +\gamma_{\rm in}\sum_l L_l\,\varrho\,L_l^\dagger\,,\end{aligned} \tag{7}$$

where we introduced the symbol $\mathcal{L}$ for the Liouvillian, denoting a linear mapping that acts on the density matrix ϱ. The Liouvillian corresponds to the linear mapping defined by the right-hand-side of the master equation. The first term describes the Hamiltonian dynamics governed

by the coherent coupling fields, the second term corresponds to the decay of the excited level and the coherences between the ground and excited levels, while the third term accounts for the incoherent population of the ground states due to the internal decay process. Even though the decay process is incoherent, it creates in general coherent superposition states because multiple decay events occur simultaneously: the step operators of Eq. (4) describe simultaneous decay events, as a consequence of the degeneracy of the upper and lower states. Moreover, this master equation doesn't preserve the norm of the density operator because it is not in the Lindblad form: without the external decay (formally setting $\gamma_{\rm ext} = 0$) the master equation would be in the Lindblad form, but the external decay describes population loss from the system under study, hence the norm of the density operator necessarily decreases. In the next section we discuss the details of our state reconstruction procedure.

III. MATHEMATICAL BACKGROUND OF THE STATE RECONSTRUCTION

The master equation (7) describes a relaxation process to some stationary state, the determination of which is the purpose of this section. To this end, we follow the derivation of ref. [52]. The solution of Eq. (7) for stationary (CW) driving field reads

$$\varrho(t) = e^{\mathcal{L}t}\,\varrho_0 = \sum_{i=1}^{64} e^{\lambda_i t}(\varrho_{\rm L}^{(i)}|\varrho_0)\,\varrho_{\rm R}^{(i)}\,, \tag{8}$$

where λ_i is the ith eigenvalue of the Liouvillan, $\varrho_{\rm L}^{(i)}$ ($\varrho_{\rm R}^{(i)}$) span the left (right) eigensystem of $\mathcal{L}$, respectively. In total there are $(2J_g+1)+(2J_e+1)$ Zeeman sublevels involved in the excitation process, hence for our choice of $J_g = 2$ and $J_e = 1$, the operator $\mathcal{L}$ acts on a 64 dimensional linear space of density matrices. The scalar product $(\square|\square)$ is evaluated as $\mathrm{Tr}\{\varrho_a\,\varrho_b\}$. In general, the left (right) hand eigenvectors do not form orthogonal sets, but they are mutually orthogonal, hence they can be chosen orthonormal

$$(\varrho_{\rm L}^{(i)}|\varrho_{\rm R}^{(j)}) = \delta_{ij}\,. \tag{9}$$

Since the master equation (7) describes a relaxation process, the norm of the density matrix cannot increase. Therefore, the real parts of the eigenvalues λ_i of $\mathcal{L}$ must be equal to or smaller than zero, i.e. $\Re(\lambda_i) \le 0$, see also [55]. Consequently, for a long enough time evolution, all terms in the series expansion of Eq. (8) which are associated with eigenvalues with negative real part vanish. Only those terms which belong to the eigenvalue zero remain. The eigenstates that belong to the eigenvalue zero are the stationary states of the Liouvillian. They are defined by the equations

$$\mathcal{L}\,\varrho_{\rm R}^{(i)} \;=\; 0\,, \tag{10a}$$

$$\varrho_{\rm L}^{(i)}\,\mathcal{L} \;=\; 0\,, \tag{10b}$$

where the indices $i = 1 \ldots N_0$ label the stationary solutions. With these eigenstates, the long-time solution of the master equation (7) is given by

$$\varrho(\infty) = \sum_{i=1}^{N_0} (\varrho_{\rm L}^{(i)}|\varrho_0)\,\varrho_{\rm R}^{(i)}\,, \tag{11}$$

In the following subsections we describe how to obtain the left- and right-hand-side stationary states of the Liouvillian.

A. The right-hand-side stationary states of the Liouvillian operator

In this section we derive the right-hand-side stationary states of the Liouvillian operator, i.e. the solutions of Eq. (10a). We begin with the decomposition of the density operator ϱ in the bare atomic basis as

$$\boldsymbol{\varrho} = \begin{bmatrix} \boldsymbol{\varrho}_{ee} & \boldsymbol{\varrho}_{eg} \\ \boldsymbol{\varrho}_{ge} & \boldsymbol{\varrho}_{gg} \end{bmatrix}\,, \tag{12}$$

where $\boldsymbol{\varrho}_{ee}$ is defined in the excited state set, $\boldsymbol{\varrho}_{gg}$ in the ground state set, and $\boldsymbol{\varrho}_{ge/eg}$ are the coherences between them. For brevity, we omit the subscript R. Using the decomposition of Eq. (12), the Eq. (10a) takes the form

$$\begin{aligned} &-\imath \begin{bmatrix} \boldsymbol{\Omega}\boldsymbol{\varrho}_{ge} - \boldsymbol{\varrho}_{eg}\boldsymbol{\Omega}^\dagger & \boldsymbol{\Delta}\boldsymbol{\varrho}_{eg} + \boldsymbol{\Omega}\boldsymbol{\varrho}_{gg} - \boldsymbol{\varrho}_{ee}\boldsymbol{\Omega} \\ -\boldsymbol{\Delta}\boldsymbol{\varrho}_{ge} - \boldsymbol{\varrho}_{gg}\boldsymbol{\Omega}^\dagger + \boldsymbol{\Omega}^\dagger\boldsymbol{\varrho}_{ee} & \boldsymbol{\Omega}^\dagger\boldsymbol{\varrho}_{eg} - \boldsymbol{\varrho}_{ge}\boldsymbol{\Omega} \end{bmatrix} \\ &-\frac{\gamma_{\rm ext}+\gamma_{\rm in}}{2}\begin{bmatrix} 2\boldsymbol{\varrho}_{ee} & \boldsymbol{\varrho}_{eg} \\ \boldsymbol{\varrho}_{ge} & \mathbf{0} \end{bmatrix} + \gamma_{\rm in}\sum_l \begin{bmatrix} \mathbf{0} & \mathbf{0} \\ \mathbf{0} & \boldsymbol{L}_l\boldsymbol{\varrho}_{ee}\boldsymbol{L}_l^\dagger \end{bmatrix} = \mathbf{0}\,. \end{aligned} \tag{13}$$

The right-hand-side stationary states cannot have components of excited states due to the radiative decay, hence $\boldsymbol{\varrho}_{ee} = \boldsymbol{\varrho}_{ge/eg} = \mathbf{0}$. It follows that Eq. (13) simplifies to

$$\begin{bmatrix} \mathbf{0} & \boldsymbol{\Omega}\boldsymbol{\varrho}_{gg} \\ -\boldsymbol{\varrho}_{gg}\boldsymbol{\Omega}^\dagger & \mathbf{0} \end{bmatrix} = \mathbf{0}\,. \tag{14}$$

This equation says that the right-hand-side stationary states of the Liouvillian are composed of the dark/stationary states of the Hamiltonian of Eq. (2). They are given by

$$\Phi_D^{(1)} \;=\; \frac{1}{\mathcal{N}_1}[0,0,0,0,-\Omega_-,0,\Omega_+,0]^T\,, \tag{15a}$$

$$\Phi_D^{(2)} \;=\; \frac{1}{\mathcal{N}_2}[0,0,0,\Omega_-^2,0,-\sqrt{6}\Omega_-\Omega_+,0,\Omega_+^2]^T. \tag{15b}$$

The stationary states depend only on the relative amplitudes of the σ_- and σ_+ components of the filter laser, and not on the absolute magnitudes of these components. There are four different ways of forming normalised density matrices from these states, a possible choice for the

right-hand-side stationary states reads

$$\varrho_{\rm R}^{(1)} = \frac{1}{\sqrt{2}}\left(|\Phi_D^{(1)}\rangle\langle\Phi_D^{(1)}| + |\Phi_D^{(2)}\rangle\langle\Phi_D^{(2)}|\right) . \quad (16a)$$

$$\varrho_{\rm R}^{(2)} = \frac{1}{\sqrt{2}}\left(|\Phi_D^{(1)}\rangle\langle\Phi_D^{(1)}| - |\Phi_D^{(2)}\rangle\langle\Phi_D^{(2)}|\right) , \quad (16b)$$

$$\varrho_{\rm R}^{(3)} = \frac{1}{\sqrt{2}}\left(|\Phi_D^{(1)}\rangle\langle\Phi_D^{(2)}| + |\Phi_D^{(2)}\rangle\langle\Phi_D^{(1)}|\right) , \quad (16c)$$

$$\varrho_{\rm R}^{(4)} = \frac{\imath}{\sqrt{2}}\left(|\Phi_D^{(1)}\rangle\langle\Phi_D^{(2)}| - |\Phi_D^{(2)}\rangle\langle\Phi_D^{(1)}|\right) , \quad (16d)$$

These states are Hermitian. They are formally identical to those density operator basis states that define the Bloch-sphere associated with a two-level system. The first one (16a) has a nonvanishing trace, while the others (16b) – (16d) are traceless.

We conclude that the Liouvillian of Eq. (7) has a four-dimensional subspace that belongs to the eigenvalue zero. We will see later that only one of the stationary states, Eq. (16a) is relevant for the state reconstruction.

B. The left-hand stationary states of the Liouvillian operator

In this section we derive the left-hand-side stationary states of the Liouvillian, i.e. the solutions of Eq. (10b). Instead of solving this equation directly, it is easier to deal with its adjungate $\mathcal{L}^\dagger\varrho_{\rm L} = 0$. The adjungate of the Liouville operator can be obtained by taking the adjungate of each of the operators that form the Liouvillian. This procedure yields

$$\mathcal{L}^\dagger\varrho = \frac{\imath}{\hbar}[H,\varrho] - \frac{\gamma_{\rm ext}+\gamma_{\rm in}}{2}(L_e\varrho + \varrho L_e) + \gamma_{\rm in}\sum_l L_l^\dagger\varrho L_l\,. \quad (17)$$

The solution of this equation is substantially more complicated than for Eq. (10a). For convenience, the linear space of the density operators $\{\varrho\}$ can be represented by vectors $\{\boldsymbol{r}\}$ with components $r_{8(i-1)+j} = (\varrho)_{i,j}$, where $(\varrho)_{i,j}$ is the matrix element of the density operator ϱ in the ordered basis

$$\{|g,-2\rangle, |g,-1\rangle, |g,0\rangle, |g,1\rangle, |g,2\rangle, |e,-1\rangle, |e,0\rangle, |e,1\rangle\}\,. \quad (18)$$

The scalar product of vectors is defined as $(\boldsymbol{r}^{(1)}|\boldsymbol{r}^{(2)}) = \sum_s r_s^{(1)*} r_s^{(2)} = {\rm Tr}\left\{\varrho^{(1)}\varrho^{(2)}\right\}$. The conjugate of the eigenvalue equation (10b) in this representation takes the form

$$\mathcal{L}^\dagger\boldsymbol{r} = \boldsymbol{0}\,, \quad (19)$$

where $\mathcal{L}^\dagger$ is the matrix representation of the adjungate Liouvillian defined by Eq. (17) in the ordered basis of Eq. (18). We solved the system of linear equations (19) using symbolic computer algebra programs, such as Mathematica [56]. The details of the procedure are presented in [57]. The result is the explicit form of four left hand side stationary states. These states together with the right hand side stationary states of Eq. (16) satisfy the orthogonality relation of Eq. (9).

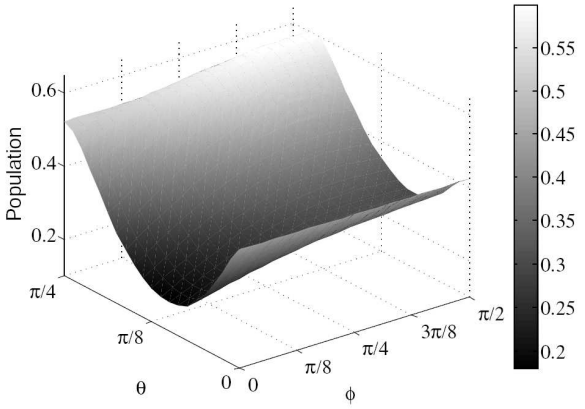

FIG. 2: The dependence of the final population left in the system on the polarization of the filter laser. The angles ϑ and φ are defined in Eq. (21). The parameters of the simulation are given in the text.

One may wonder why it is not sufficient to solve the equations numerically, but necessary to find the algebraic form of the left-hand-side stationary states as well. The reason is that our reconstruction procedure relies on the linear independence of some of the elements of the left-hand-side stationary states of the Liouvillian, which can be studied by means of their explicit algebraic representation.

IV. STATE RECONSTRUCTION

With the solutions of the right-hand-side and left-hand-side eigenvectors available we have all ingredients in hand for discussing the state reconstruction procedure. As we showed in the previous section, the final state of the system is given by Eq. (11) with $N_0 = 4$ for a CW coherent driving field. In the beginning of Sec. II it was stated that after the pumping process reaches a stationary state, the remaining population should be measured. The measured population can be calculated by taking the trace of the final density matrix $\varrho(\infty)$ of Eq. (11). Inserting the right-hand-side density matrices of Eq. (16) into Eq. (11) and calculating the trace of the sum yields

$$\sqrt{2}(\varrho_{\rm L}^{(1)}|\varrho_0) = P_f\,, \quad (20)$$

because $\varrho_{\rm R}^{(2-4)}$ are traceless. Equation (20) is linear for the nine components of the initial density matrix ϱ_0. For a fixed initial state ϱ_0, the actual value of P_f depends on $\varrho_{\rm L}^{(1)}$ which in turn depends on the atomic parameters $\gamma_{\rm in}$ and $\gamma_{\rm ext}$. Moreover, they depend on the polarization and intensity of the coherent driving field. The polarization state of the driving field can be characterized by two

angles: the angle ϑ describes the relative amplitude of the σ_+ and σ_- components of the field, while φ describes their relative phase. In terms of these parameters, the coupling strengths $\Omega_\pm$ are given by

$$\begin{aligned} \Omega_+ &= \Omega e^{\imath\varphi}\cos\vartheta\,, \\ \Omega_- &= \Omega\sin\vartheta\,. \end{aligned} \tag{21}$$

When ϑ and φ are varied, the population P_f of Eq. (20) will also vary. In Fig. 2 we plot P_f as a function of ϑ and φ, for the initial density matrix $[\varrho_{11},\varrho_{33},\varrho_{55},\varrho_{13},\varrho_{15},\varrho_{35}] = [0.5, 0.1, 0.4, 0.2236\,\imath, -0.4472\,\imath, 0.1+0.05\,\imath]$. In this state the coherence is maximal between ϱ_{11} and ϱ_{33} and between ϱ_{11} and ϱ_{55}, but non-maximal between ϱ_{33} and ϱ_{55}, hence it represents the main features of a general density matrix. The other parameters of the system are given in Sec. V A.

A series of population measurements for different settings of the polarization parameters yield a set of linear equations that connects the matrix elements of the density matrix with the measured populations. In the matrix-vector notation, this linear equation reads

$$\boldsymbol{S}\boldsymbol{r}_0 = \boldsymbol{P}_f\,, \tag{22}$$

where $\boldsymbol{r}_0$ is a column vector composed of the elements of the density matrix ϱ_0, $\boldsymbol{r}_0 = [(\varrho_0)_{1,1},(\varrho_0)_{3,3},(\varrho_0)_{5,5},(\varrho_0)_{1,3},(\varrho_0)_{3,1},(\varrho_0)_{1,5},(\varrho_0)_{5,1},(\varrho_0)_{3,5},(\varrho_0)_{5,3}]^T$. Each row of the matrix $\boldsymbol{S}$ is formed of the corresponding elements of the left-hand-side stationary state $\varrho_{\rm L}^{(1)}$ for a different setting of the driving laser field. Finally, $\boldsymbol{P}_f$ is a column vector which consists of the measured populations. We call the matrix $\boldsymbol{S}$ *sampling matrix* for the initial state. The vector $\boldsymbol{r}$ is nine-dimensional, and in principle we can have an arbitrary number n of different polarization settings for which the population is measured, hence $\boldsymbol{S}$ is $n\times 9$ dimensional. The reconstruction of the initial density matrix ϱ_0 requires the inversion of the Eq. (22). This equation is invertible if the sampling matrix $\boldsymbol{S}$ is a rank nine matrix, i.e. the number of rows of $\boldsymbol{S}$ is at least nine ($n\geq 9$), and $\boldsymbol{S}$ has nine nonzero singular values. One may try to construct a sampling matrix just by inserting a series of polarization values and checking that the obtained matrix fulfil the previous criteria. However, using the algebraic form of the left-hand-side stationary state $\varrho_{\rm L}^{(1)}$ one may show that those matrix elements which are used in the construction of the sampling matrix $\boldsymbol{S}$ are linearly independent functions of the polarization parameters ϑ and φ, see [57]. This means, that it is indeed always possible to chose the measurement parameters such that the sampling matrix is invertible. Moreover, we have a great freedom to choose the polarization of the filter laser during the design of the measurement process.

Now we discuss briefly the reason of the restriction of the initial state space to the $M_g=-2,0,2$ magnetic levels of the $J_g=2$ state: The full state space consists of 5 magnetic sublevels, hence the density matrix is characterised by 25 real parameters. In order to retrieve all 25 parameters, the sampling matrix $\boldsymbol{S}$ should be a rank 25 matrix. It turns out that by using $\sigma_\pm$ and π polarized components of the filter laser, and varying the direction of propagations as well, the number of independent elements of $\varrho_L^{(1)}$ is less than 25. Therefore, our reconstruction scheme for the $M_g=-2,0,2$ magnetic sublevels cannot be extended to the full 5 level state space by adding the π polarized component and varying the polarization state of the filter laser.

In the next section we study in detail the accuracy of the state reconstruction procedure with respect to different choice of laser field polarizations and pulse shapes.

V. ACCURACY ANALYSIS

In this section we study the impact of different choices of field polarizations and pulse shape on the accuracy of our state reconstruction procedure.

A. Rectangular pulse

The analytic consideration of the previous sections assumes a rectangular pulse shape. In practice this means a rapid rise-up time compared to the period of the coherent oscillations between the ground and excited levels and to the life-time of the excited level. Such a pulse envelope can be applied in the case of trapped, well localized atoms. In order to construct the sampling matrix $\boldsymbol{S}$ of Eq. (22) one may choose an equally spaced set of polarization parameters as defined by Eq. (21) $\varphi\in[0,\pi/2]$ and $\vartheta\in[0,\pi/2]$. However, this might not be the optimal choice from the state reconstruction point of view: as we described at the end of the previous section, in order to find the original matrix elements of ϱ_0 from the measured populations, we have to invert Eq. (22). The accuracy of inversion depends on the condition number of the matrix in the linear equation which is defined by the ratio of its largest and smallest singular value [58].

We have worked out specific numerical examples for the metastable neon atom. The parameters of our simulations are: the decay rates of the excited level $^3P_1$ are $\gamma_{\rm in}=1.1\times10^7{\rm s}^{-1}$ and $\gamma_{\rm ext}=4.378\times10^7{\rm s}^{-1}$, the Rabi frequency $\Omega=5\times10^7{\rm s}^{-1}$, and the detuning $\Delta=10^7{\rm s}^{-1}$. Using only nine series of measurements, in case of the uniform distribution of the polarization parameters the condition number of the obtained sampling matrix is 2733. However, we performed a numerical optimization of the condition number: The optimization procedure minimized the condition number of the sampling matrix by varying the polarization parameters of the driving laser field. This procedure yielded a sampling matrix with a condition number of 22. Using the optimized set of polarizations, one obtains the sampling matrix of Eq. (22), which is more stable numerically and can be inverted

more accurately. An efficient method for the inversion is the least square fit, such as the algorithm `zgglse` of `LAPACK` [59], or the built in functionality of Mathematica or Matlab.

B. Gaussian pulse

We will show below that our state reconstruction procedure can be applied in experiments where the filter laser has a Gaussian envelope: In a typical atomic beam experiment after the atoms leave the source and the beam is collimated, they cross the manipulation and/or measuring laser beams at right angle. In the local coordinate system of the atoms, they experience pulsed laser beams with Gaussian envelope. In a typical experiment for metastable neon [51], the atomic velocity distribution is Gaussian with mean velocity $v = 800\,\mathrm{ms}^{-1}$ and width of $300\,\mathrm{ms}^{-1}$ (FWHM). Assuming $d = 1\,\mathrm{mm}$ laser-beam cross section (FWHM width), the resulting effective time-dependent Rabi frequency is given by $\Omega(t) = \Omega\exp(-t^2/2\tau^2)$ with $\tau = d/v = 1.25\,\mu\mathrm{s}$, which is nearly 70 times longer than the lifetime of the excited state, approx. $0.0182\,\mu\mathrm{s}$.

Here we cannot apply the basic equation (20) directly to construct the sampling matrix. Instead, one can build the sampling matrix by numerically solving the master equation (7) for a basis in the density matrix space: In our case the initial state of the system can be expanded in the density operator basis $\{|g,i\rangle\langle g,j|\}$ with $i,j = -2,0,2$, so that $\varrho_0 = \sum_{ij}(\varrho_0)_{i+3,j+3}\,|g,i\rangle\langle g,j|$, where the density matrix elements $(\varrho_0)_{i,j}$ are expressed in the ordered basis of Eq. (18). The time evolution of the system subject to the driving laser field is given by the weighted sum of the time-evolved flip operators

$$\varrho(t) = \sum_{i,j}(\varrho_0)_{i,j}\,R_{i,j}(t)\,, \tag{23}$$

where $R_{i,j}(t)$ is the solution of the master equation (7) with initial state $|g,i\rangle\langle g,j|$, i.e. $R_{i+3,j+3}(0) = |g,i\rangle\langle g,j|$ for $i,j = -2,0,2$. After the system has reached the steady state, the population left in the dark subspace is given by

$$P_f = \sum_{i,j}\mathrm{Tr}\{R_{i,j}(\infty)\}\,(\varrho_0)_{i,j}\,. \tag{24}$$

Comparing this equation with the defining equation (22) of the sampling matrix we see that the quantities $\mathrm{Tr}\{R_{i,j}(\infty)\}$ are the corresponding elements of the sampling matrix, more precisely, they give the elements of one of the rows of the sampling matrix $\boldsymbol{S}$.

Below we summarize the steps of the construction of the sampling matrix:

1. Set the polarization of the driving field (filter laser) by choosing a (ϑ_l,φ_l) pair, and insert the resulting coupling strengths of Eq. (21) into the master equation (7).

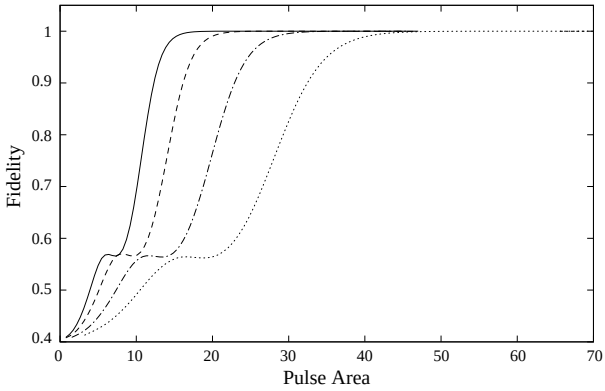

FIG. 3: The fidelity of the state reconstruction as a function of the area $\sqrt{2\pi}\Omega\tau$ of a Gaussian filter laser pulse $\Omega\exp(-t^2/2\tau^2)$ for the state of Fig. 2. The fidelity is defined by Eq. (25). The curves correspond to the pulse width of $\tau = 1.25\mu$s (dotted); $\tau = 0.625\mu$s (dashed-dotted); and $\tau = 0.3125\mu$s (dashed), respectively. For reference we plotted the fidelity curve for a rectangular pulse of duration 1μs (solid line). The pulse areas are varied by increasing the peak Rabi frequency Ω.

2. Evolve numerically the elements of the density matrix basis $\{|g,i\rangle\langle g,j|\}$ $(i,j = -2,0,2)$ with the master equation. The time evolution of the basis elements can be calculated in the ordered basis of Eq. (18).

3. After reaching a steady state $(t = T)$, calculate the trace of the obtained matrices $R_{i,j}(T)$, i.e. $Q_{i,j} = \mathrm{Tr}\{R_{i,j}(T)\}$.

4. The l-th row of the sampling matrix S is given by $[Q_{1,1},Q_{3,3},Q_{5,5},Q_{1,3},Q_{3,1},Q_{1,5},Q_{5,1},Q_{3,5},Q_{5,3}]$

5. Repeat this procedure from step 1 until a sufficient number of rows of the sampling matrix $\boldsymbol{S}$ is obtained.

6. After constructing the sampling matrix, the state reconstruction can be performed exactly in the same way as in case of the rectangular pulse.

To demonstrate the usage and efficiency of the state reconstruction procedure with Gaussian filter laser envelope, we performed a numerical simulation: the system was again the metastable neon, the filter laser parameters are defined in the beginning of this subsection. In Fig. 3 the fidelity of the state reconstruction is shown as a function of the pulse area of the filter laser.

The fidelity $\mathcal{F}$ of the reconstruction is defined through the relation

$$\mathcal{F} = \frac{\mathrm{Tr}\{\varrho_f\,\varrho_0\}}{\sqrt{\mathrm{Tr}\{\varrho_f^2\}\mathrm{Tr}\{\varrho_0^2\}}}\,. \tag{25}$$

The normalization is necessary, because for any non-pure state ϱ, $\mathrm{Tr}\{\varrho^2\} < 1$, hence without the normalization the

fidelity would be smaller than unity even if the reconstruction was perfect.

Returning back to Fig. 3, one can see that for small pulse area the fidelity is low, and increasing the pulse area the fidelity saturates to unity. This behaviour is the consequence of the coherent pumping process: for small pulse are the system cannot scatter enough photons to relax fully into the dark subspace. By increasing the pulse area, the system performs more cycles among the ground and excited states, hence more photons are scattered from the excited state leading to more complete relaxation into the dark subspace.

We plotted the fidelity–curve for three different values of the pulse width. One can see that the shorter the pulse, the more rapid the convergence to unit fidelity.

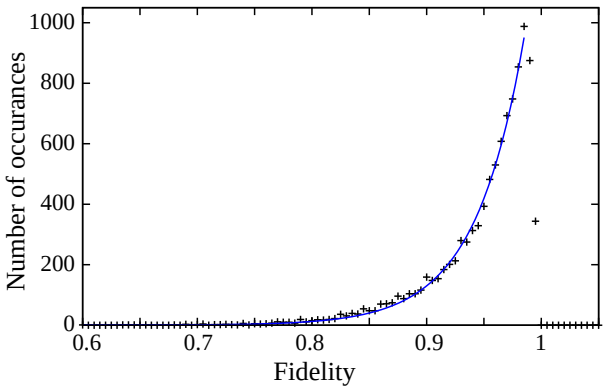

FIG. 4: Histogram of the fidelity of the reconstruction for the state of Fig. 2: the horizontal axis is the fidelity of the reconstruction, whereas the vertical axis is the number of events, when the fidelity of the reconstruction falls in the small interwall $[\mathcal{F}_i, \mathcal{F}_i + \delta\mathcal{F}]$. The fideliy $\mathcal{F}$ is defined by Eq. (25). The continuous line represents a fitted exponential curve.

C. Precision of the population retrieval

In a real experiment, the value of the experimental parameters is known to some finite precision. In case of our state reconstruction procedure the main source of uncertainty is the inaccuracy of the adjustment of the polarization and phase of the filter laser defined in Eq. (21): we assume that the angles ϑ and φ are random parameters with Gaussian distribution. The actual value of these parameters determines $\varrho_L^{(1)}$ which in turn determines the measured population through the relation of Eq. (20).

We modelled the population measurement as follows: in a simulation the values of ϑ and φ were chosen randomly around the optimized mean values. The width of the Gaussian distributions were chosen 0.5 degree ($\pi/360$ rad). Then the measurable populations were calculated using Eq. (20). Finally, applying the reconstruction formula of Eq. (22), the initial quantum state of the system was reconstructed. The sampling matrix $\boldsymbol{S}$ was calculated for the fixed, optimized filter laser polarizations and phases. Due to the random distribution of the polarizations and phases used for the calculation of populations, the obtained densiy matrix elements have also random distribution.

In Fig. 4 we display the result of the simulation: The parameters of the simulation were the same as for Fig. 2. Based on 10.000 runs, the histogram shows the number of events when the fidelity of the state reconstruction falls in the range $[\mathcal{F}_i, \mathcal{F}_i+\delta\mathcal{F}]$, where $\mathcal{F}_i = i\delta\mathcal{F}$ and $\delta\mathcal{F} = 1/200$. The distribution of the fidelity is well approximated with an exponential one of the form $N_0 \exp((\mathcal{F} - \mathcal{F}_0)/\Delta\mathcal{F})$, with $\mathcal{F}_0 \approx 0.985$, $\Delta\mathcal{F} \approx 0.0427$, and $\mathcal{F} \leq \mathcal{F}_0$. We conclude that for achievable accuracy of the adjustment of the filter laser polarizations and phases, the state reconstruction procedure retrieves the quantum state of the system with high fidelity.

VI. SUMMARY

In this paper we addressed the problem of retrieving the quantum state of a degenerate quantum system: we worked out a reconstruction procedure for the quantum state in the magnetic sublevels $M = -2, 0, 2$ of a $J = 2$ angular momentum state. Our scheme is based on a coherent pumping technique, which populates the dark states defined by the filter laser and some population is pumped out of the system as well. The population left in the dark subspace is measured in a subsequent step. It is shown that by varying the polarization state of the filter laser, enough information can be retrieved from the system through the population measurements to reconstruct the initial state.

We provided a recipe to perform the state reconstruction from a set of measured populations. Furthermore, we analyzed the accuracy of the reconstruction procedure with respect to the choice of the filter laser polarizations: We showed that there is an optimal choice for the set of polarizations which maximizes the accuracy of the state reconstruction.

The basic reconstruction scheme is worked out for a rectangular envelope of the filter laser. We showed that the procedure works with high fidelity for a filter laser with Gaussian envelope as well.

Finally we studied the fidelity of the reconstruction procedure with respect to the inaccuracy in the adjustment of the polarization and phase of the filter laser. We found that 0.5 degree uncertainty in the angles of the polarization and phase leads to an exponential distribution for the fidelity of the state reconstruction. The distribution has small enough width so that it is very likely that the reconstruction procedure retrieves the state of the system with high fidelity.

In conclusion, we presented a reconstruction procedure for retrieving the quantum state of a degenerate quan-

tum system with high actuary. The scheme can be implemented straightforwardly using well established technologies, hence we assume that it will be implemented in many laboratories where the coherent control of quantum systems is studied.

Acknowledgements

The authors are grateful to B.W. Shore for useful discussion. ZK acknowledge the support of the Research Fund of the Hungarian Academy of Sciences under contracts T043287 and T049234, moreover, the support of the EU Transfer of Knowledge project CAMEL.

[1] T.F. Gallagher, *Rydberg Atoms*, (Cambridge University Press, Cambridge, 1994).
[2] T.C. Weinacht, J. Ahn, and P.H. Bucksbaum, Nature **397**, 233 (1999).
[3] J. M. Raimond, M. Brune, and S. Haroche, Rev. Mod. Phys. **73**, 565 (2001).
[4] M. Shapiro and P. Brumer, Rep. Prog. Phys. **66**, 859 (2003).
[5] E. Arimondo, Prog. Optics **35**, 257 (1996).
[6] A.B. Matsko, O. Kocharovskaya, Y. Rostovtsev, G.R. Welch, A.S. Zibrov, and M.O. Scully, Adv. At. Mol. Opt. Phys. **46**, 191 (2001).
[7] M. Fleischhauer, A. Imamoglu, and J. P. Marangos, Rev. Mod. Phys. 77, 633 (2005).
[8] N.V. Vitanov, M. Fleischhauer, B.W. Shore, and K. Bergmann, Adv. At. Mol. Opt. Phys. **46**, 57 (2001).
[9] N.V. Vitanov, T. Halfmann, B.W. Shore, and K. Bergmann, Ann. Rev. Phys. Chem. **52**, 763 (2001)
[10] M. Shapiro and P. Brumer, Phys. Rep. **425**, 195 (2006).
[11] R.J. McLean, R.J. Ballagh and D.M. Warrington, J. Phys. B **19**, 3477 (1986).
[12] D. Suter, Phys Rev A. **46**, 344 (1992).
[13] A. Weis, V.A. Sautenkov and T.W. Hansch, Phys Rev A **45**, 7991 (1992).
[14] A.S. Parkins, P. Marte, P. Zoller and H.J. Kimble, Phys. Rev. Lett. **71**, 3095-3102 (1993).
[15] W. Hanle, Z. Phys. **30**, 93 (1924).
[16] G. Breit, Rev. Mod. Phys. **5**, 91 (1933).
[17] W. Rasmussen, R. Schneider, and H. Walther, Opt. Commun. **12**, 315 (1974).
[18] A. S. Parkins, P. Marte, P. Zoller, O. Carnal and H. J. Kimble, Phys. Rev. A **51**, 1578-1596 (1995).
[19] W. Lange and H. J. Kimble, Phys. Rev. A **61**, 063817 (2000).
[20] F. Mattinson, M. Kira, S. Stenholm, J. Mod. Optics 48, 889 (2001).
[21] O. Kocharovskaya and Ya.I. Khanin, JETP Lett. **48**, 630 (1988).
[22] S.E. Harris, Phys. Rev. Lett. **62**, 1033 (1989).
[23] M.O. Scully, S.-Y. Zhu, and A. Gavrielides, Phys. Rev. Lett. **62**, 2813 (1989).
[24] S. E. Harris, J. E. Field, and A. Imamou, Phys. Rev. Lett. **64**, 1107 (1990).
[25] M. Fleischhauer, M.D. Lukin, Phys. Rev. Lett. **84**, 5094 (2000).
[26] C. Liu, Z. Dutton, C.H. Behroozi, L.V. Hau, Nature **409**, 490 (2001).
[27] M.D. Eisaman, A. Andre, F. Massou, M. Fleischhauer, A.S. Zibrov, M.D. Lukin, Nature **438**, 837 (2005).
[28] M. Jain, H. Xia, G. Y. Yin, A. J. Merriam, and S. E. Harris Phys. Rev. Lett. **77**, 4326 (1996).
[29] J. H. Eberly and A. Rahman, and R. Grobe, Phys. Rev. Lett. **76**, 3687 (1996).
[30] A. Eilam, A. D. Wilson-Gordon, and H. Friedmann Phys. Rev. A **73**, 053805 (2006).
[31] C.K. Law and J. Eberly, Opt. Exp. **2**, 368 (1998).
[32] N.V. Vitanov, Z. Kis, and B.W. Shore, Phys. Rev. A **68**, 063414 (2003).
[33] J. Oreg, F. T. Hioe, J.H. Eberly, Phys. Rev. A **29**, 690 (1984); J. R. Kuklinski, U. Gaubatz, F. T. Hioe, and K. Bergmann, Phys. Rev. A **40**, 6741 (1989); U. Gaubatz, P. Rudecki, S. Schiemann, and K. Bergmann, J. Chem. Phys. **92**, 5363 (1990).
[34] P. Marte, P. Zoller and J.L. Hall, Phys. Rev. A **44**, R4118 (1991).
[35] J. Lawall and M. Prentiss, Phys. Rev. Lett. **72**, 993 (1994).
[36] L.S. Goldner, C. Gerz, R.J.C. Spreeuw, S.L. Rolston, C.I. Westbrook, W.D. Phillips, P. Marte, and P. Zoller, Phys. Rev. Lett. **72**, 997 (1994).
[37] M. Weitz, B.C. Young, and S. Chu, Phys. Rev. Lett. **73** 2563 (1994).
[38] R.G. Unanyan, M. Fleischhauer, B.W. Shore, and K. Bergmann, Opt. Commun. **155**, 144 (1998).
[39] H. Theuer, R.G. Unanyan, C. Habscheid, K. Klein, and K. Bergmann, Opt. Express **4**, 77 (1999).
[40] R.G. Unanyan, B.W. Shore, and K. Bergmann, Phys. Rev. A **59**, 2910 (1999).
[41] R.G. Unanyan, B.W. Shore, and K. Bergmann, Phys. Rev. A **63**, 043401 (2001).
[42] A. Karpati and Z. Kis, J. Phys. B **36**, 905 (2003).
[43] Z. Kis, A. Karpati, B.W. Shore, and N.V. Vitanov, Phys. Rev. A **70**, 053405 (2004).
[44] Z. Kis, N.V. Vitanov, A. Karpapti, C. Barthel, K. Bergmann, Phys. Rev. A **72**, 033403 (2005).
[45] T.C. Weinacht, J. Ahn, and P.H. Bucksbaum, Phys. Rev. Lett. **80**, 5508 (1998).
[46] M. Dantus, M.J. Rosker, and A.H. Zewail, J. Chem. Phys **87**, 2395 (1987).
[47] T.J. Dunn, I.A. Walmsley, and S. Mukamel, Phys. Rev. A **74**, 884 (1995).
[48] I.Sh. Averbukh, M. Shapiro, C. Leichte, and W.P. Schleich, Phys. Rev. A **59**, 2163 (1999).
[49] N.V. Vitanov, B.W. Shore, R.G. Unanyan, and K.

Bergmann, Opt. Commun. **179**, 73 (2000).
[50] N.V. Vitanov, J. Phys. B **33**, 2333 (2000).
[51] F. Vewinger, M. Heinz, R. Garcia Fernandez, N.V. Vitanov, K. Bergmann, Phys. Rev. Lett. **91**, 213001 (2003).
[52] A. Karpati, Z. Kis, and P. Adam, Phys. Rev. Lett. **93**, 193003 (2004).
[53] J. R. Morris and B. W. Shore, Phys. Rev. A **27**, 906 (1983).
[54] The amplitudes $\Omega_{\pm}$ are the reduced matrix elements of the transiton dipole operator which can be calculated using the Wigner-Eckart theorem. For a detailed explanation see e.g. R.N. Zare, *Angular Momentum*, (John Wiley & Sons, Inc., 1988).
[55] Due to the choice of the ground level energy, $E_g = 0$, the stationary states are time independent, therefore, the imaginary part of the eigenstates of the Liouvillian associated with stationary states are also zero, i.e. $\Im(\lambda_i = 0)$.
[56] S. Wolfram, *The Mathematica Book* (Cambridge University Press and Wolfram Media, Champaign, 1999).
[57] C. Barthel, *Diploma work: Manipulation und Tomografie kohärenter Überlagerungen entarteter Quantenzustände*, (Kaiserlautern, 2005).
[58] W.H. Press, S.A. Teukolsky, W.T. Vetterling, B.P. Flannery, *Numerical Recipes in C* (Cambridge University Press, 2002).
[59] E. Anderson, Z. Bai, C. Bischof, S. Blackford, J. Demmel, J. Dongarra, J. Du Croz, A. Greenbaum, S. Hammarling, A. McKenney, D. Sorensen, *LAPACK Users' Guide*, (Society for Industrial and Applied Mathematics, 1999).